

TNO report
FEL-96-A053

A bulk model to predict optical turbulence in the marine surface layer

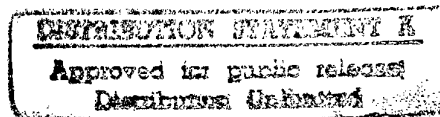
TNO Physics and Electronics
Laboratory

Oude Waalsdorperweg 63
PO Box 96864
2509 JG The Hague
The Netherlands

Phone +31 70 374 00 00
Fax +31 70 328 09 61

Date
April 1996

Author(s)
G.J. Kunz



Classification
Classified by : W. Pelt
Classification date : 19 November 1996

Title : Ongerubriceerd
Managementuitreksel : Ongerubriceerd
Abstract : Ongerubriceerd
Report text : Ongerubriceerd
Appendices A - E : Ongerubriceerd

All rights reserved.
No part of this publication may be
reproduced and/or published by print,
photoprint, microfilm or any other means
without the previous written consent of
TNO.

In case this report was drafted on
instructions, the rights and obligations of
contracting parties are subject to either the
Standard Conditions for Research
Instructions given to TNO, or the relevant
agreement concluded between the
contracting parties.

Submitting the report for inspection to
parties who have a direct interest is
permitted.

© 1996 TNO

Copy no : 7
No of copies : 52
No of pages : 73 (incl appendices,
excl RDP & distribution list)
No of appendices : 5

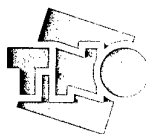
All information which is classified according to Dutch regulations shall be treated by the
recipient in the same way as classified information of corresponding value in his own
country. No part of this information will be disclosed to any party.

The classification designation Ongerubriceerd is equivalent to Unclassified, Stg.
Confidentieel is equivalent to Confidential and Stg. Geheim is equivalent to Secret.

DTIC QUALITY INSPECTED 3

The TNO Physics and Electronics Laboratory is part of
TNO Defence Research which further consists of:

TNO Prins Maurits Laboratory
TNO Human Factors Research Institute



Netherlands Organization for
Applied Scientific Research (TNO)

19970130 028

Managementuittreksel

Titel : A bulk model to predict optical turbulence in the marine surface layer
Auteur(s) : Ir. G.J. Kunz
Datum : april 1996
Opdrachtnr. : A94KM786
IWP-nr. : 766.4
Rapportnr. : FEL-96-A053

Aanleiding

Moderne electro-optische sensoren zijn in staat om over honderden kilometers waarnemingen uit te voeren, zoals vanuit satellieten. Echter, in de onderste laag van de atmosfeer zal tengevolge van transmissieverliezen, contrast-reductie en turbulentie dit bereik aanzienlijk kleiner zijn. De transmissieverliezen en de contrastreductie worden hoofdzakelijk bepaald door verstrooiing van de straling door atmosferische aerosolen en geven aanleiding tot een tijdsafhankelijke verslechtering van de informatie. Enige correctie is mogelijk. Turbulentie echter, met name optische turbulentie, geeft aanleiding tot tijdsafhankelijke intensiteitsfluctuaties en beeldvervalsing, waardoor de prestaties van de sensor ver onder de specificaties kunnen komen. Onder operationele omstandigheden kan dit, tengevolge van verkeerde interpretatie of te late beslissing, ernstige gevolgen hebben. Aangezien het op dit moment vrijwel uitgesloten moet worden geacht om de door turbulentie verstoorte beelden betrouwbaar te corrigeren met de snelheid waarmee de beelden worden gegenereerd, moet bij tactische beslissingen rekening worden gehouden met de atmosferische omstandigheden waaronder optische turbulentie een beperkende factor zal worden.

Doel

In dit rapport wordt een model beschreven en uitgewerkt waarmee het mogelijk is om de micrometeorologische eigenschappen in de oppervlaktelaag van de maritieme atmosfeer te voorspellen op basis van standaard meteorologische waarnemingen. De numerieke waarden van de parameters die het model levert worden gebruikt om een schatting te maken van effecten tengevolge van optische turbulentie.

Korte omschrijving

De omvangrijke set van vergelijkingen waarmee de micrometeorologie in de maritieme oppervlaktelaag beschreven wordt, kan iteratief opgelost worden met als randvoorwaarden de actuele windsnelheid, luchttemperatuur, -vochtigheid en -druk en watertemperatuur. Daarnaast worden empirische waarden gebruikt van de uitwisselingscoëfficiënten voor de fluxen van impuls, warmte en vocht. Tenslotte wordt gebruik gemaakt van verschillende fysische constanten. De gevonden

oplossing levert de primaire parameters waarmee de verticale profielen van windsnelheid, temperatuur en vochtigheid berekend kunnen worden alsmede de fluxen van impuls, warmte en vocht. Aan de hand van deze gegevens, in combinatie met een model van de atmosferische brekingsindex, wordt het verticale profiel van de brekingsindex berekend, hetgeen noodzakelijk is voor het voorspellen van o.m. 'ducting' en voor het ondersteunen van 'ray tracing' programma's. De meest essentiële parameter voor het voorspellen van optische turbulentie, de structuurfunctie-parameter voor de brekingsindex C_n^2 , wordt eveneens berekend. Dit rapport geeft een complete en overzichtelijke beschrijving van het model inclusief vele tussenresultaten (in de vorm van grafieken) die van belang zijn voor micrometeorologisch onderzoek.

Conclusies

Met behulp van het beschreven model krijgt TNO-FEL de beschikking over een eigen micrometeorologisch model dat gebruik maakt van de meteorologische invoerparameters die op verschillende hoogten gemeten kunnen zijn. Tevens kan de gebruiker een keuze maken of hij de berekeningen zal baseren op een windsnelheidsafhankelijke 'drag'-coëfficiënt of een wrijvingssnelheidsafhankelijke ruwheidslengte voor windsnelheid. Het model levert zowel de parameters voor het berekenen van de verticale profielen van wind, temperatuur, vochtigheid en de structuurfunctie parameter voor de brekingsindex alsmede de parameters voor het berekenen van de fluxen van impuls, warmte en vocht. Het is verrassend om te ervaren dat bij een dergelijke omvangrijke set vergelijkingen binnen een beperkt aantal (8 of minder) iteraties de nauwkeurigheid van de oplossing beter is dan 10^{-3} . De 'interne' betrouwbaarheid van het model is getest door herberekening van de ingevoerde meteorologische gegevens aan de hand van de door het model geleverde parameters. De resultaten verschillen niet meer dan 10^{-10} . De prestaties van het model zijn tevens getoetst aan de hand van ca. 500 berekeningen van verschillende parameters onder verschillende condities uit de open literatuur. Overeenkomstige berekeningen, uitgevoerd met het beschreven model, komen uitstekend overeen (beter dan 1%) met de gepubliceerde resultaten.

De berekende waarden van de brekingsindex van lucht komen overeen met twee andere onafhankelijke modellen.

Berekeningen hebben aangetoond dat voor windsnelheden boven 4 m/s, de optische turbulentie (intensiteitsvariatie en versmering; Engelse termen: 'scintillation' en 'blur',) voornamelijk bepaald wordt door het temperatuurverschil tussen lucht en water en in veel mindere mate door de windsnelheid en het vochtprofiel. Opvallend hierbij is dat het teken van het temperatuurverschil van ondergeschikt belang is, zodat onder 'stabiele' condities er wel degelijk turbulentie-effecten kunnen optreden. Slechts onder 'neutrale' en 'bijna-neutrale' condities is de turbulentie beperkt. Optische turbulentie neemt slechts zwak toe met toenemende windsnelheid. Intensiteitsvariatie en versmering in het infrarood zijn beduidend minder dan in het zichtbare deel van het EM-spectrum. Bij sterke turbulentie zal tengevolge van

(scintillatie)verzadiging er geen voorkeur bestaan voor een bepaalde golflengte. Voor zover bekend, treden bij versmering geen verzadigingseffecten op.

Aanbevelingen

Bij de keuze van een waarnemingssysteem verdient het aanbeveling om de invloed van atmosferische turbulentie in aanmerking te nemen. In het infrarood kunnen de effecten tengevolge van atmosferische turbulentie aanzienlijk minder zijn dan in het zichtbare deel van het EM-spectrum.

Het beschreven model voorspelt effecten van atmosferische turbulentie op basis van statistische verwachtingen (gemiddelden en standaarddeviaties). Hoewel het in principe onmogelijk is om het gedrag in de tijd te voorspellen, bijvoorbeeld voor het simuleren van door turbulentie vervormde beelden, is het wel mogelijk om de tijdsafhankelijkheid te simuleren aan de hand van modelspectra.

Verder is het aan te bevelen om het model uit te breiden met een model voor 'ray tracing' teneinde refractie-effecten te kunnen voorspellen.

Contents

1.	Introduction	6
1.1	Background	6
2.	Surface layer bulk model	8
2.1	Introduction	8
2.2	Micrometeorology	9
2.3	Solution Scheme	18
2.4	Exchange coefficients	19
2.5	Structure function parameters	21
2.6	Model Verification and Results	22
3.	Optical parameters	32
3.1	Introduction	32
3.2	Refractive index of air	32
3.3	Optical turbulence	35
3.4	Scintillation	39
3.5	Blurring	42
3.6	mage motion	44
4.	Summary and conclusions	45
5.	Recommendations	47
6.	Acknowledgement	48
7.	References	49
8.	Signature	54
	Appencides	
A	List of symbols	
B	Tables with numerical results	
C	Short sensitivity analysis	
D	Fluxes of momentum, heat and water vapor as a function of wind speed and air-sea temperature difference	
E	Specific humidity versus relative humidity and air temperature	

1. Introduction

This report describes a micrometeorological model for the marine surface layer. Based on standard (bulk) meteorological observations it predicts the vertical profiles of the wind speed, temperature and humidity, turbulent fluxes of momentum, heat and water vapor and other micrometeorological parameters. The results are used to estimate the vertical profiles of the index of refraction $n(z)$ and the structure function parameter, $C_n^2(z)$. These profiles are used for predicting atmospheric refraction effects (sub- and super refraction, mirages) and turbulence effects (scintillation, blurring and image dancing) respectively. The results obtained are compared with data available from literature and with experimental data.

1.1 Background

For high quality, long range imaging systems, state of the art optical systems are required that combine high resolution with high sensitivity. Under operational conditions, the quality of the image can seriously be degraded due to atmospheric effects. Four major effects are distinguished: 1. transmission losses, 2. contrast reduction, 3. turbulence and 4. refraction. Transmission losses decrease the radiance that can be received from a target due to absorption and scattering by atmospheric constituents. As a result, the signal-to-noise ratio decreases and in the ultimately the signal from the target cannot be discriminated from the system noise. Contrast reduction is caused by the addition of the scattered background radiation to the radiance from the target. For large distances, the radiance received from the target becomes comparable to the radiance received from the background. Although transmission losses and contrast reduction are both caused by scattering of atmospheric constituents (aerosols and molecules) and do not reduce the resolution of the image in principle. Optical and infrared turbulence is caused by the irregular distribution of the atmospheric refractive index which, in turn, is induced by the irregular distribution of temperature and humidity along the path of observation. Turbulence causes scintillation, blurring, and image dancing and thus decreases the spatial resolution of the image.

Because the dynamic range in the signal strength of the detection unit is generally larger than that of the display unit, contrast reduction in the image can partly be compensated using (on line) image processing. Effects of turbulence, on the other hand, result not only in a loss of contrast but also in a loss of resolution due to blurring and image dancing. Moreover, the image can be distorted due to the vertical distribution of the refractive index. Correction for effects due to turbulence and refraction is difficult if not impossible. Therefore, any module in a technical decision aid that can help to predict effects due to atmospheric optical turbulence can contribute to a better understanding of the phenomena in the image and will contribute to a higher detection rate.

Atmospheric turbulence is either generated by wind (shear) and/or by convective processes due to vertical temperature and/or humidity gradients. In daily life, turbulence is visible in the curly patterns of stack plumes, flags, ribbons and water in rivers but also in the irregular shape of cumulus clouds and in a kettle of boiling water. Via a cascade process, the large patterns split in smaller and smaller eddies without losing energy. This interval is called the inertial subrange and varies from about the height above the surface to several millimeters. Finally, the motion is damped by molecular viscosity. Statistical analysis of the sizes shows that the eddy sizes within the inertial subrange are distributed according to the famous $-5/3$ power law (Kolmogorov spectrum), see e.g. Panofski and Dutton (1984).

Eddies have different motion, composition and/or air densities compared to their environment. As a result, the eddies must be traced with dedicated sensors, dependent on the requirements of the user. For example, there are different sensors for measuring wind speed variations, temperature variations and humidity variation but there are also sensors that can measure turbulent fluctuations of other atmospheric gases such as carbon dioxide. Note that the different physical parameters of the eddies do not necessarily correlate.

A direct method to quantify turbulence (assuming that the processes are isotropic) is to measure the mean square of the difference of the physical parameter of interest as a function of the distance between the two sensors. For example the structure function of the physical parameter x is calculated from $\langle [X(r) - X(r+R)]^2 \rangle$, in which the $\langle \rangle$ brackets indicate ensemble averaging. It is common practice to symbolize this expression with $D_{xx}(R)$. Using dimensional analysis, it can be shown that within the inertial subrange $D_{xx}(R)$ is a function of the distance R and of the atmospheric condition which is expressed in the structure function parameter, C_x^2 . Thus the structure function can also be written as $D_{xx}(R) = C_x^2 R^{2/3}$. For optical turbulence in the atmosphere, the structure function parameter for the refractive index, C_n^2 , is the controlling parameter to predict turbulence effects such as scintillation, blurring and image dancing.

In this report, a first attempt is presented to model optical and IR turbulence in the marine surface layer (first 50 to 100 m above the sea surface) from the actual weather condition measured with standard meteorological sensors which are not necessarily at the same height. The model is based on methods that are commonly used in micrometeorology for the estimation of statistically reliable turbulent fluxes of momentum, heat and water vapor and on values of the exchange coefficients for the above mentioned quantities. These coefficients are available from literature. They are based on many field experiments. This so called surface layer bulk model provides the vertical profiles for wind speed, temperature and humidity and other micrometeorological parameters such as fluxes, roughness lengths, scaling parameters and stability. These results are essential for modelling other atmospheric effects such as the profiles for the refractive index and the refractive index structure function parameter.

2. Surface layer bulk model

2.1 Introduction

This chapter deals with a set of equations describing atmospheric turbulence in the marine surface layer using standard meteorological observations as input. In addition the 10 m neutral exchange coefficients for the fluxes of interest are used as input parameters. The set of equations can be solved iteratively to obtain the necessary parameters for the calculation of the atmospheric stability, the roughness lengths, scaling parameters and fluxes of momentum, heat and water vapor as well as the vertical profiles of wind speed, temperature and humidity. From these parameters the vertical profiles of the refractive index and of the structure function parameter can be calculated.

Micrometeorology in the marine surface layer is among others concerned with vertical turbulent fluxes of momentum, heat and water vapor as well as with other constituents such as CO₂ or aerosols. Thus, how much wind energy is coupled to the waves and how much heat and/or water vapor is exchanged between the air and the underlying water surface. In the last decades, many theoretical and laboratory tests have lead to a better understanding of turbulence. Much of this work is also applicable to atmospheric turbulence where wind speed, air-sea temperature difference (ASTD) and the air humidity are the main driving forces. However, fluxes are difficult to measure directly. Therefore, equations have been derived which describe that part of the micrometeorology in terms of actual meteorological observations. Micrometeorology, in turn, provides equations for the vertical profiles of wind speed, temperature and humidity in the surface layer. Nowadays, many of these equations are generally accepted and can be found in standard text books such as Tennekes and Lumley (1972), Businger (1973), Panofsky and Dutton (1984) and Stull (1988).

In this chapter the equations will be presented as the start for our model. For an extensive description and derivation of these equations, one is referred to the books mentioned above and/or other referenced literature.

Presentation and explanation of the complex problem of atmospheric turbulence is a laborious task that can be approached in many ways. This report starts with a postulation of the equations that describe the fluxes of momentum, heat and water vapor in terms of standard meteorological observations at two different heights. All heights are in the marine surface layer. In the next step, the equations for the vertical profiles for wind speed, temperature and water vapor are given and discussed. The two sets of equations, in combination with some additional parameters, form a closed set that will be solved to acquire the parameters that are necessary to predict turbulence and the vertical profiles for wind speed, temperature and humidity in the marine surface layer. Relevant relations between the different parameters are presented and discussed. The obtained results are used to calculate the structure function parameters for temperature and humidity that in

turn form the basics for the structure function parameter for the refractive index that will be discussed in the next chapter. In the last section of this chapter, results from a number of model calculations are presented in graphical form as illustrations of stability, scaling parameters, roughness lengths, the refractive index structure function parameter, scintillation and blurr all as a function of wind speed and air-sea temperature difference. Also vertical profiles of wind speed, air temperature, humidity and refractive index structure function are presented under different conditions.

2.2 Micrometeorology

The vertical momentum flux, also called stress, is the force per unit area exerted by the wind field on the surface. It can be expressed in the product of the gradient, the exchange coefficient for momentum flux and the air density as shown in equation (2.1). The exchange coefficient is also called the drag coefficient. To be consistent with equations (2.2) and (2.3), the square of the gradient of the wind speed has explicitly been written as a product. By definition, the downward directed momentum flux is positive.

$$\tau = \rho C_D (U_z - U_s)(U_z - U_s) \quad (2.1)$$

where:

- τ = momentum flux in N/m^2 ;
- ρ = air density in kg/m^3 ;
- C_D = exchange coefficient for momentum or drag coefficient;
- U_z = wind speed at height z in m/s ;
- U_s = wind speed near the sea surface at $z = z_{ou}$ in m/s ;
- z_{ou} = roughness length for wind speed in m .

The vertical turbulent sensible heat flux is the amount of heat transferred per unit area due to vertical gradients in the temperature and the wind speed. The expression for the heat flux is given in equation (2.2). The sign has been chosen such that upward directed flux is positive (a warm surface leads to a positive flux).

$$H = -c_p \rho C_H (U_z - U_s)(\Theta_z - \Theta_s) \quad (2.2)$$

where:

- H = sensible heat flux in W/m^2 ;
- c_p = specific heat at constant pressure in J/(kg.K) ;
- ρ = air density in kg/m^3 ;
- C_H = exchange coefficient for heat or Stanton number;
- U_z = wind speed at height z in m/s ;
- U_s = wind speed near the sea surface in m/s ;
- Θ_z = potential temperature at height z , in K ;
- Θ_s = potential temperature near the surface in K .

The potential temperature Θ is invariant with altitude. It is the temperature of an air parcel if brought adiabatically (without adding or removing energy) to a reference height or pressure. Normally, the reference height is the surface. The potential temperature is a conservative quantity and can be calculated using equation (2.3).

$$\Theta = T \left(\frac{P_o}{P} \right)^{R_g / m c_p} \quad (2.3)$$

where:

- T = temperature in K;
- P = pressure in Pa;
- P_o = reference pressure in Pa;
- c_p = specific heat of air at constant pressure in J/(kg.K);
- R_g = universal gas constant in J/(kmol.K);
- m = apparent molecular weight of air in kmol.

The numerical value of the exponent is about 0.286.

The pressure at a certain height can be calculated from the hydrostatic equation:

$$dP = -g \rho dz \quad (2.4)$$

where:

- g = acceleration due to gravity in m/s^2 ;
- dP = change in pressure in Pa;
- ρ = density of air in kg/m^3 ;
- dz = change in height in m.

The numerical value of the vertical pressure lapse rate, dP/dz , is about -10 Pa/m. As a result, the temperature lapse rate under standard pressure and temperature (1013.25 hPa and 15 °C) is about 0.01°C per meter.

The vertical turbulent water vapor flux is the amount of water vapor transferred per unit area due to a gradient in the specific humidity in combination with a vertical gradient in the wind speed. An expression for the vertical turbulent water vapor flux is given in equation (2.5a). The sign has been chosen such that a positive flux is directed upwards.

$$E = -\rho C_E (U_z - U_s) (q_z - q_s) \quad (2.5a)$$

The water vapor flux can also be expressed in terms of heat that is necessary to evaporate this amount of water. In that case the water vapor flux is expressed in the so called latent heat flux by multiplication of the water vapor flux by the latent heat of vaporization, L , as shown in equation (2.5b).

$$H_e = -\rho L_v C_E (U_z - U_s) (q_z - q_s) \quad (2.5b)$$

where:

- E = water vapor flux in $\text{kg}/(\text{m}^2 \cdot \text{s})$;
- H_e = latent heat flux in W/m^2 ;
- L_v = latent heat of vaporization in J/kg ;
- ρ = air density in kg/m^3 ;
- C_E = exchange coefficient for water vapor or Dalton number;
- U_z = wind speed at height z in m/s ;
- U_s = wind speed near the sea surface in m/s ;
- q_z = specific humidity at height z , in kg/kg ;
- q_s = saturation specific humidity near the sea surface in kg/kg .

(The saturation specific humidity is calculated from an analytical approach of the saturation water vapor pressure given by Byers, 1959 and the saturation relative humidity. Above the sea surface, the saturation relative humidity is about 98 %. Over sweet water this is 100 %.)

Equations 2.1 to 2.5 can be used to calculate the fluxes of momentum, heat and water vapor from bulk meteorological observations, provided that the exchange coefficients are known. However, the exchange coefficients are seldom available because they depend on the meteorological condition and vary with the height above the sea surface. In addition, the drag coefficient is a function of the geographic location. Therefore, and for the reason of comparison, experimentalists have converted their exchange coefficients to the 10 m standard height under neutral conditions (neutral stability means an adiabatic lapse rate and no convection). These exchange coefficients are published as $C_{DN}(10)$, $C_{HN}(10)$ and $C_{EN}(10)$ or simply as C_{DN} , C_{HN} and C_{EN} in which the subscript 'n' refers to neutral. See e.g. Smith (1988) and Geernaert (1990).

Based on the eddy correlation technique, the fluxes of momentum, sensible heat and water vapor are expressed as ensemble averages of the products of the vertical wind speed fluctuations with respectively fluctuations of the horizontal wind speed, temperature and specific humidity.

$$\tau = -\rho \langle w' u' \rangle \quad (2.6)$$

$$H = \rho c_p \langle w' \theta' \rangle \quad (2.7)$$

$$E = \rho \langle w' q' \rangle \quad (2.8a)$$

$$H_e = \rho L_v \langle w' q' \rangle \quad (2.8b)$$

For normalisation purposes, see e.g. Hill (1989a), the micrometeorology defines a set of scaling parameters which are directly derived from the ensemble averages. For the purpose of symmetry, we write:

$$u_* \equiv -\frac{\langle w' u' \rangle}{u_*} \quad (2.9)$$

$$\theta_* \equiv -\frac{\langle w' \theta' \rangle}{u_*} \quad (2.10)$$

$$q_* \equiv -\frac{\langle w' q' \rangle}{u_*} \quad (2.11)$$

where:

- u_* = scaling wind speed or friction velocity in m/s;
- θ_* = scaling temperature in K;
- q_* = scaling humidity in kg/kg.

An alternative set of equations for the fluxes in terms of the scaling parameters is found by substitution of (2.9), (2.10) and (2.11) respectively in (2.6), (2.7) and (2.8). This results in:

$$\tau = \rho u_*^2 \quad (2.12)$$

$$H = -\rho c_p u_* \theta_* \quad (2.13)$$

$$E = -\rho q_* u_* \quad (2.14a)$$

$$H_e = -\rho L_v q_* u_* \quad (2.14b)$$

Although the series of equations (2.6) to (2.14) does not seem to directly contribute to solving our problem, it will be shown later that these scaling parameters are essential for the calculation of the equivalent meteorological conditions at the 10 m standard height under neutral conditions and the neutral exchange coefficients. Thus we force the solution to agree with the given neutral exchange coefficients.

The equations for the vertical profiles of wind speed, temperature and humidity are postulated. (see e.g. the standard work of Panofsky and Dutton, 1984).

The wind speed as a function of altitude can be written as:

$$(U_z - U_o) = \frac{u_*}{k} \left[\ln\left(\frac{z}{z_{ou}}\right) - \psi_m\left(\frac{z}{L}\right) \right] \quad (2.15)$$

where:

- U_z = wind speed as a function of height in m/s;
- U_o = per definition zero but to be consistent with (2.16) and (2.17) this value has been introduced;
- u_* = friction velocity in m/s; can also be described as $u_*^2 = \tau / \rho$;
- k = von Kármán constant, commonly used value is 0.4;
- z = height of interest in m;
- z_{ou} = roughness length for wind speed in m;
- L = Monin-Obukhov length in m; see (2.18)
- ζ = expression for the stability of the atmosphere $\zeta = z / L$;
- $\psi_m(\zeta)$ = correction function for stability (Panofsky and Dutton, 1984)
 - for $\zeta > 0$, $\psi_m(\zeta) = 5\zeta$ and
 - for $\zeta < 0$, $\psi_m(\zeta) = \ln \left[\frac{(1+x^2)}{2} \frac{(1+x)^2}{2} \right] + 2 \arctan(x) + \frac{\pi}{2}$.
- with $x = (1 - 16\zeta/L)^{1/4}$.

Note: The roughness length for wind speed is not a physical quantity but a mathematical quantity to indicate the height where the wind speed vanishes. In a similar way, the roughness lengths for temperature and humidity are defined in (2.16) and (2.17).

The vertical profile of the potential temperature is expressed as:

$$(\Theta_z - \Theta_o) = \frac{\theta_*}{k} \left[\ln\left(\frac{z}{z_{ot}}\right) - \psi_t\left(\frac{z}{L}\right) \right] \quad (2.16)$$

where:

- Θ_z = potential temperature at height z , in K;
- Θ_o = (potential) temperature near the sea surface in K;
- θ_* = scaling potential temperature, $\theta_* = -H / \rho \cdot c_p \cdot u_*$;
- z_{ot} = roughness length for temperature in m;
- $\psi_t(\zeta)$ = correction function for temperature (Panofsky and Dutton, 1984)
 - for $\zeta > 0$, $\psi_h(\zeta) = 5\zeta$ and
 - for $\zeta < 0$, $\psi_h(\zeta) = 2 \ln \left[\frac{1}{2} (1 + \sqrt{1 - 16\zeta}) \right]$.

The profile of the specific humidity is given by equation (2.17).

$$(Q_z - Q_o) = \frac{q_*}{k} \left[\ln\left(\frac{z}{z_{oq}}\right) - \psi_q\left(\frac{z}{L}\right) \right] \quad (2.17)$$

where:

- Q_z = specific humidity at height z , in kg/kg;
 - Q_s = specific humidity near the sea surface in kg/kg;
 - q_* = scaling specific humidity, $q_* = -E / \rho \cdot u_*$;
 - z_{oq} = roughness length for specific humidity in m;
 - $\psi_q(\zeta)$ = correction function for humidity (Panofsky and Dutton, 1984).
- $$\psi_q(\zeta) = \psi_t(\zeta)$$

The Monin-Obukhov length L , is a mathematical quantity that is used to describe the stability of the atmosphere. Physically, it can be interpreted as the height above the surface where the turbulent mixing caused by buoyancy effects due to temperature and humidity gradients becomes comparable with the mixing by mechanical turbulence generated by wind effects. Within the surface layer, the Monin-Obukhov length is independent of height and must be determined from measurements as close to the surface as possible (Panofsky and Dutton, 1984).

L is related to the several micrometeorological parameters and has been published in various equations. Many of them can be reduced to one form. Three different appearances are presented in (2.18a) to (2.18c). The literature is not clear about the height at which the temperature must be taken for the calculation of the Monin-Obukhov length e.g. Davidson et al. (1981), Anderson and Smith (1981), Large and Pond (1982), Smith (1980, 1989), Fairall et al. (1980, 1990), Geernaert et al. (1986, 1987), Geernaert (1988), Hill (1989), Edson et al. (1991), Hill, Ochs and Wilson (1992), Anderson (1993) and Yelland et al. (1994). Because a certain value is required for the model, we will follow the work of Smith (1988) and Donelan (1990) in which the virtual temperature (2.19) of the surface is used. For consistency of the used symbols, we will express this as the virtual potential temperature. This is allowed because the reference pressure P_o is determined at the mean sea level, and thus the surface virtual potential temperature Θ_{vs} is equal to the surface virtual temperature T_{vs} . The virtual potential temperature at the surface Θ_v , is calculated in two steps. First the virtual temperature is calculated using equation (2.19) and subsequently the virtual potential temperature is obtained from equation (2.3).

$$L = \frac{\Theta_{vs} u_*^2}{g k \theta_{v*}} \quad (2.18a)$$

$$L = \frac{\Theta_{vs} u_*^3}{g k [\theta_* (1 + 0.608 Q_s) + 0.608 \Theta_s q_*]} \quad (2.18b)$$

$$L = - \frac{c_p \rho u_*^3 \Theta_{vs}}{g k H (1 + 0.07 / B)} \quad (2.18c)$$

where B is the ratio of the sensible heat flux to the latent heat flux, or the Bowen Ratio $B = H / H_e$. The factor 0.07 is an approximation of $0.608 T c_p / L_v$. The virtual temperature, T_v , is a mathematical tool that translates the influence of water vapor on the density of air (the molecular weight of water vapor is smaller than that of dry air) to a temperature dependence of the density. The virtual temperature can be written as:

$$T_v = T \frac{1}{1 - \frac{e}{P} + \frac{m_w}{m_d} \frac{e}{P}} \quad (2.19a)$$

where:

- T = actual temperature of the air parcel in K;
- T_v = virtual temperature of the air parcel in K;
- e = partial water vapor pressure in Pa;
- m_w = molecular weight of water vapor in kmol;
- m_d = molecular weight of 'dry air' in kmol;
- P = total air pressure in Pa.

Using the definition of the specific humidity $Q = M_w / (M_d + M_w)$, in combination with the expression for the water vapor partial pressure $e = (M_w / m_w) / (M_w / m_w + M_d / m_d)$, the virtual temperature can be written in an approximation that is useful for our application:

$$T_v \approx T (1 + 0.608 Q) \quad (2.19b)$$

The virtual potential temperature-scaling-parameter θ_{vs} , that is used in equation (2.18a), is derived from the virtual scaling temperature followed by a correcting for altitude. The total derivative of (2.19b) is:

$$t'_v = t' + 0.608 T q' + 0.608 Q t' \quad (2.20a)$$

with $t'_v = dT_v$, $q' = dQ$ and $t' = dT$.

For the calculation of the Monin-Obukhov length, the temperatures and humidities are taken from the surface, thereby avoiding the questions from which heights the temperature and the specific humidity should be taken. Thus the virtual potential temperature fluctuations can easily be expressed as

$$\theta'_v = \theta' + 0.608 \Theta q' + 0.608 Q \theta' \quad (2.20b)$$

Ensemble averages with the vertical wind variations w' and normalizing with the friction velocity u_* leads to:

$$\theta_{v*} = \theta_* (1 + 0.608 Q) + 0.608 q_* \Theta \quad (2.20c)$$

Because the specific humidity Q is of the order of 0.01 this can be simplified by:

$$\theta_{v*} = \theta_* + 0.608 q_* \Theta \quad (2.20d)$$

At this point, the pool of equations collected thus far can be solved (using only the meteorological parameters at the heights of observation and the neutral exchange coefficients). The key for the inversion lies in rewriting (2.15) under neutral conditions while assuming that the roughness length is a function of the surface only. This results in:

$$U_{10N} = \frac{u_*}{k} \ln \left(\frac{10}{z_{ou}} \right) \quad (2.21)$$

and because

$$C_{DN} = \left[\frac{u_*}{U_{10N}} \right]^2 \quad (2.22)$$

an explicit expression for the roughness length z_{ou} can directly be obtained by eliminating the quotient u_* / U_{10N} from (2.21) and (2.22). For a uniform format in agreement with (2.31) and (2.32) we write:

$$C_{DN} = \frac{k^2}{\ln \left(\frac{10}{z_{ou}} \right) \ln \left(\frac{10}{z_{ou}} \right)} \quad (2.23)$$

thus

$$z_{ou} = 10 \exp \left(\frac{-k}{\sqrt{C_{DN}}} \right) \quad (2.24)$$

Substitution of z_{ou} in equation (2.15) with the measured wind speed at the height of the sensor provides the value for the friction velocity u_* . Because the Monin-Obukhov length, L , can be calculated using (2.18), the vertical profile for wind speed is defined.

It is interesting to note that for the solution of the vertical wind profile also Charnock's equation, (2.25), can be used instead of the neutral drag coefficient C_{DN} . A brief history on Charnock's equation can be found in Geernaert (1990).

According to Smith (1988) we write:

$$z_{ou} = \frac{0.011 u_*^2}{g} + \frac{0.11 \nu}{u_*} \quad (2.25)$$

where:

$$\begin{aligned} \nu &= \text{dynamic viscosity, } 1.4 \cdot 10^{-6} \text{ m/s;} \\ g &= \text{acceleration due to gravity, } 9.81 \text{ m/s}^2. \end{aligned}$$

Other values for the constants are given e.g. by Wu (1982), Rojas (1993) and Makin *et al.* (1995). The solution is somewhat different because first z_{ou} and u_* must be solved from (2.25) and (2.15). Subsequently, the neutral exchange coefficient can be calculated e.g. by using (2.23). Note that neither z_{ou} nor u_* can be written explicitly from these equations.

In the next step, the roughness length for temperature will be derived assuming that in the marine surface layer this parameter does not vary with stability. Following the method applied for wind speed, cf. equation (2.21), the temperature difference under neutral conditions can be written as:

$$(\Theta_{10N} - \Theta_s) = \frac{\theta_*}{k} \ln \left(\frac{10}{z_{ot}} \right) \quad (2.26)$$

From (2.2), (2.7) and (2.10) we can write for the neutral exchange coefficient for temperature:

$$C_{HN} = \frac{\theta_*}{(\Theta_s - \Theta_{10N})} \cdot \frac{u_*}{U_{10N}} \quad (2.27)$$

or, after substitution of (2.22):

$$C_{HN} = \frac{\theta_*}{(\Theta_s - \Theta_{10N})} \sqrt{C_{DN}} \quad (2.28)$$

Finally, z_{ot} can be solved from (2.26) and (2.28). This results in:

$$z_{ot} = 10 \exp \left(\frac{-k \sqrt{C_{DN}}}{C_{HN}} \right) \quad (2.29)$$

Because of the symmetry in the equations for the water vapor flux and the sensible heat flux, the roughness length for water vapor becomes, in analogy with (2.29):

$$z_{oq} = 10 \exp \left(\frac{-k \sqrt{C_{DN}}}{C_{EN}} \right) \quad (2.30)$$

Of course, from (2.23), (2.29) and (2.30), the exchange coefficients can explicitly be expressed in terms of the roughness lengths. This results in the neutral Stanton number:

$$C_{HN} = \frac{k^2}{\ln\left(\frac{10}{z_{ot}}\right) \ln\left(\frac{10}{z_{ou}}\right)} \quad (2.31)$$

and in the neutral Dalton number for water vapor flux:

$$C_{EN} = \frac{k^2}{\ln\left(\frac{10}{z_{oq}}\right) \ln\left(\frac{10}{z_{ou}}\right)} \quad (2.32)$$

2.3 Solution Scheme

Although at this point all the ingredients are available to solve for u_* , θ_* and q_* and thus for the fluxes, explicit analytical expressions cannot be derived because the solutions for the scaling parameters are implicitly defined in the argument of stability terms via the Monin-Obukhov length in equations (2.18) to (2.20). Therefore, it is necessary to solve the set of equations iteratively. The sequence of the equations within the iterative loop is summarized in Table 2.1. The inter-relation between the different parameters has been indicated with arrows. A downward arrow indicates that the estimated value of the parameter is required in the procedure indicated at the end of the arrow. An upwards directed arrow indicates that the estimated value will be used in a next iteration.

Table 2.1: Overview of the sequence of equations and the inter-relation of the different parameters that is applied to solve the set of micrometeorological equations. Downward directed arrows indicate the forward use of a calculated parameter whereas upward directed arrows indicate intermediate results that are re-used in the next iteration. The numbers refer to the equations in section 2.2.

Input: $T_a(z_r)$, $RH(z_r)$, $U(z_u)$, $P(z_p)$, T_s
and implicitly

$$C_{DN}(U_{10N}), C_{HN} \text{ and } C_{EN}.$$

Guess: u_* , θ_* , q_* , U_{10N}

Loop:

step	forward	equation	backward	see
1		$L(T_{vs}, u_*, \theta_{v*}, q_*, \Theta)$		(2.18)
2		$z_{ou}(u_*) / C_{DN}(U_{10N})$		(2.25)/(2.23)
3		$C_{DN}(U_{10N}) / z_{ou}(C_{DN})$		(2.22)/(2.24)
4		$u_*[U(z_u), z_u, z_{ou}, L, \psi_m(z_u / L)]$		(2.15)
5		$U_{10N}(u_*, C_{DN})$		(2.21)
6		$C_{HN}(-)$		(-)
7		$z_{ot}(C_{HN}, C_{DN})$		(2.29)
8		$\theta_*[\Theta_a, T_s, z_{ot}, L, \psi(z_t / L)]$		(2.16)
9		$C_{EN}(-)$		(-)
10		$z_{oq}(C_{EN}, C_{DN})$		(2.30)
11		$q_*[Q_a, Q_s, z_{oq}, z_r, L, \psi(z_r / L)]$		(2.17)

Output: u_* , θ_* , q_* , L , z_{ou} , z_{ot} , z_{oq}

2.4 Exchange coefficients

The set of equations that has been presented in the previous sections will be solved using the actual meteorological condition and the neutral exchange coefficients C_{DN} , C_{HN} and C_{EN} . The first set can be considered as the external boundary for the model whereas the exchange coefficients can be considered as the internal boundary which is not intended to be controlled by the user. In this section the numerical values for the exchange coefficients are presented.

Neutral exchange coefficient for momentum or drag coefficient

Experiments have shown that the neutral drag coefficient, C_{DN} , depends on the wind speed, the sea state and the type of water (e.g. sea or open ocean). See e.g. Large and Pond (1981), Smith *et al.* (1992). Many of these data have been reviewed and summarized by Geernaert (1990). From this work, we adopt the following practical values for different conditions:

$$C_{DN} = (0.75 + 0.067 U_{10N}) \cdot 10^{-3}, \text{ average value} \quad (2.33a)$$

$$C_{DN} = (0.58 + 0.085 U_{10N}) \cdot 10^{-3}, \text{ North Sea, tower} \quad (2.33b)$$

$$C_{DN} = (0.43 + 0.097 U_{10N}) \cdot 10^{-3}, \text{ North Sea} \quad (2.33c)$$

$$C_{DN} = (0.61 + 0.063 U_{10N}) \cdot 10^{-3}, \text{ Atlantic, buoy} \quad (2.33d)$$

Neutral exchange coefficient for sensible heat or Stanton number

Values for the neutral exchange coefficients for heat and water (Stanton numbers) have been published by several authors:

$$C_{HN} = 1.1 \cdot 10^{-3} \quad (\text{Davidson et al. 1978}) \quad (2.34a)$$

$$C_{HN} = 1.13 \cdot 10^{-3} \quad (\text{Large and Pond, 1982) unstable} \quad (2.34b)$$

$$C_{HN} = 0.66 \cdot 10^{-3} \quad (\text{Large and Pond, 1982) stable} \quad (2.34c)$$

$$C_{HN} = 1.0 \cdot 10^{-3} \quad (\text{Smith 1988}) \quad (2.34d)$$

$$C_{HN} = 1.18 \cdot 10^{-3} \pm 0.19 \quad (\text{Smith et al., 1995}) \quad (2.34e)$$

Neutral exchange coefficient for water vapor or Dalton number

$$C_{EN} = 1.27 \cdot 10^{-3} \pm 0.26 \quad (\text{Anderson and Smith, 1981) neutral} \quad (2.35a)$$

$$C_{EN} = (0.55 + 0.083 U_{10N}) \cdot 10^{-3} \quad (\text{Anderson and Smith, 1981}) \quad (2.35b)$$

$$C_{EN} = 1.15 \pm 10^{-3} \quad (\text{Large and Pond, 1982) unstable} \quad (2.35c)$$

$$C_{EN} = 1.2 \cdot 10^{-3} \quad (\text{Smith, 1988}) \quad (2.35d)$$

$$C_{EN} = 1.11 \cdot 10^{-3} \pm 0.14 \quad (\text{Smith et al., 1995}) \quad (2.35e)$$

In our model, we use the values mentioned in (2.33b), (2.34d) and (2.35d).

For the alternative model that is based on the roughness length for the wind speed instead of on the neutral drag coefficient, we use the values mentioned in equation (2.25).

2.5 Structure function parameters

The ultimate goal for our model is to evaluate tools to estimate the structure function parameter for the refractive index, C_n^2 . This parameter is controlled by structure function parameters for temperature and humidity C_T^2 , C_q^2 and by the covariance structure function C_{Tq} which, in turn, are derived from the scaling temperature t_* , the scaling humidity q_* , the height above the surface and some empirical functions. Basically, the structure functions follow the Monin-Obukhov similarity theory (e.g. Fairall and Larsen, 1986) and can be described by the general function $C_x^2 = x_* z^{-2/3} f_x(z/L)$. Thus:

$$C_T^2 = z^{-2/3} t_*^2 f_1(z/L) \quad (2.36)$$

$$C_{Tq} = z^{-2/3} T_* q_* f_2(z/L) \quad (2.37)$$

$$C_q^2 = z^{-2/3} q_*^2 f_3(z/L) \quad (2.38)$$

Expressions for the empirical functions f_1 , f_2 and f_3 can be found in literature. For f_1 , expressions have been published a.o. by Fairall, Schacher and Davidson et al. (1980), Davidson (1981), Kunkel and Walters (1983), Fairall and Larsen (1986), Hill (1989), Thierman and Kohnle (1989), Hill and Ochs (1992b) and Hill, Ochs and Wilson (1992). However, all these authors refer in turn to Wyngaard, Izumi and Collins (1971). Davidson et al. (1978) tested Wyngaard's model over the ocean. An ad hoc, alternative expression for f_1 can be found in Hill, Ochs and Wilson (1992). For this work, we suggest to apply also the generally expressions for f_1 , where $\zeta = z/L$:

$$f_1(\zeta) = \begin{cases} 4.91(1-7.0\zeta)^{-2/3} & , \text{ for } \zeta < 0. \\ 4.9(1+2.4\zeta)^{2/3} & , \text{ for } \zeta > 0. \end{cases} \quad (2.39)$$

Because only one expression, (2.40), is known for f_2 from Wyngaard and Lemone (1980) which was determined over land in the free convection limit it is suggested to calculate the coherence function C_{Tq} from the structure function parameters C_T^2 and C_q^2 as suggested by a.o. Fairall, Schacher and Davidson (1980), Davidson *et*

al. (1981), Kohsiek and Herben (1983), Hill (1989) and Hill, Ochs and Wilson (1992) using equation (2.39).

$$f_2(\zeta) \approx 0.74 f_1(\zeta) \quad (2.40)$$

For the covariance structure function, Kohsiek (1982a+b) and Hill (1989) assumed:

$$C_{Tq} = \sqrt{C_T^2 C_q^2} \quad (2.41)$$

For f_3 , we suggest to apply the expressions from Fairall, Schacher and Davidson (1980) that are based on measurements over the ocean.

$$f_3(\zeta) = A f_1(\zeta) \quad (2.42)$$

in which A can either be taken from Wyngaard and LeMone (1980), Fairall, Schacher and Davidson (1980) or from Kohsiek (1982), respectively proposing the values 0.6, 0.8 and 0.84. We suggest to apply a value of 0.6 as given by Davidson *et al.* (1981).

The structure function parameters are also coupled to the structure functions. For instance for temperature $D_T(r) = C_T^2 r^{2/3}$ in which $l_o < r < L_o$. The parameter l_o is the inner scale of turbulence (the smallest turbulent eddies in the Kolomogorov spectrum) defined by $l_o = (\nu^3 / \varepsilon)^{1/4}$ with ν the kinematic viscosity. Eddies smaller in size are converted to heat due to the viscosity. For smaller eddies, the structure function is defined as $D_T(r) = C_T^2 l_o^{-4/3} r^2$. For temperature, the smallest eddies are given by $l_o = 5.8 (D^3 / \varepsilon)^{1/4}$, in which D is the diffusivity of heat in air (see e.g. Beeland, 1993). For the case of this project, the smallest size of the eddies will be assumed to be described by the viscosity.

2.6 Model Verification and Results

This section gives some background information on the procedures followed to solve the set of equations that has been presented in the previous section. The internal consistency of the model has been tested by comparison of the calculated bulk meteorological data using the micrometeorological equations with the input meteo data. In addition, the results of one of the models have been verified against data available from literature. Some results of the model are presented in graphical form.

It has been shown in the previous section that the set of equations describing the micrometeorological quantities in the marine surface layer can be solved. The input parameters for the solution are wind speed, air temperature and air humidity at a given height from within the surface layer (not necessarily from the same height), and the sea surface temperature. The model provides all the parameters

that are required to calculate fluxes of momentum, heat and water vapor as well as the parameters to calculate the vertical profiles of wind speed, temperature and humidity in the surface layer. In addition, the system provides essential parameters to predict optical turbulence such as the stability, the scaling temperature and the scaling humidity. However, the complexity of the equations is such that the parameters of interest cannot explicitly be written in an analytical form as was shown in Table 2.1 of section 2.3. Two different solutions can be provided by the model. One solution is based on the assumption of a wind speed dependent neutral drag coefficient $C_{DN}(10)$, the other is based on a friction velocity controlled roughness length z_{ou} . The two models provide different results but the difference is small as will be shown in the figures of this section.

The kernel of the model has been programmed such that the iterative loop ends when the three scaling parameters u_* , t_* and q_* are within a relative accuracy of better than 10^{-3} . This occurs for most of the situations within a few (less than 8) iterations both for stable and for unstable situations. Under conditions of low wind speeds and strong stratification (very stable conditions) the solution leads to a singularity in the Monin-Obukhov length. This is confirmed by the results from Smith (1988).

Internal calibration

The model uses the actual bulk meteorological parameters and the neutral exchange coefficients. Although it is possible to adapt the coefficients to the location of interest and/or to the actual conditions, these coefficients have been set to a default value. The model has been tested with wind speed from 0 to 36 m/s, air-sea temperature-differences (ASTD) from -20 to +20 °C, relative humidities from 50 and 95 %, a fixed water temperature of 10 °C and a fixed atmospheric pressure of 1013.25 hPa. The internal consistency of the model has been tested by comparison of the input meteorological data with the data computed to predict the vertical profiles of wind speed, temperature and humidity. Test runs have shown that within the range of conditions mentioned above, the relative accuracy of the model based on C_{DN} is better than $5 \cdot 10^{-11}$ for wind speed, better than $2 \cdot 10^{-10}$ for air temperature and better than $5 \cdot 10^{-14}$ for humidity. The relative accuracies of the model based on z_{ou} are better than $3 \cdot 10^{-11}$, $2 \cdot 10^{-10}$ and $2 \cdot 10^{-14}$ for the respective parameters. We therefore conclude that the micrometeorological parameters produced by the model, such as the roughness lengths and stability length, are reliable.

External validation

The performance of the model based on z_{ou} has been validated with numerical results from Smith (1988). Smith provided eight tables with exchange coefficients and wind speed ratios (U_{10}/U_1 , U_{10}/U_2 , U_{10}/U_5 and U_{10}/U_{20}) under 492 different conditions. The results of our model for the same conditions are presented in Appendix B. For the majority of the situations (98 %), the calculated results compare excellent with Smith's. Under only a few conditions, which were all near

a strong gradient in the results, the maximum value of the difference is 4 %. It seems that rounding of intermediate results are the cause for these differences. The excellent comparison of the results is indicative for the reliability of the model. The results of our model based on C_{DN} are also presented in Appendix B.

A second test was carried out by comparing the relation between the dimensionless temperature structure parameter $C_\theta^2 z^{2/3} / \theta_*^2$ and the stability term z/L in a similar way as Davidson *et al.* (1978). Actually, the relation between the scaling temperature θ_* and the Monin-Obkhov length L , both from the model, is tested because C_θ is directly coupled to the stability through equation (2.36). To test the relation, the wind speed was varied from 0.5 to 25 m/s, the air-sea temperature-difference was varied from -20 to +20 °C and height above the surface was varied from 1 to 20 m. Thus the comparison was carried out both under various meteorological conditions and at various heights. In addition, the calculations were carried out both for the model based on C_{DN} and the model based on z_{ou} . The results provided by the model, which are shown in Figure 2.1, are in excellent agreement with those from Davidson.

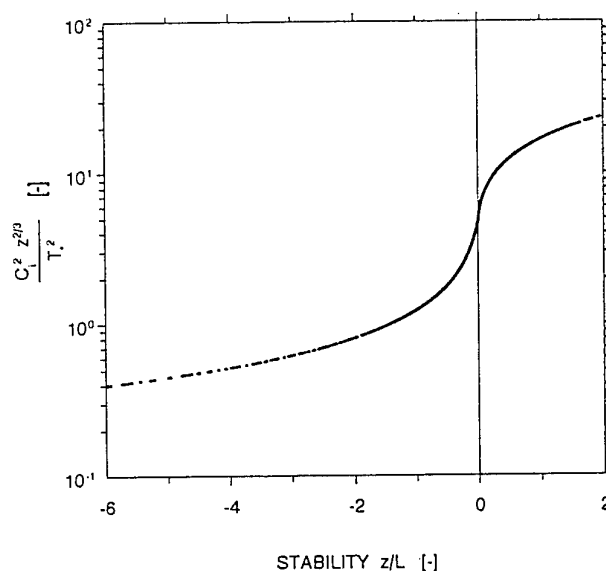


Fig. 2.1: $C_\theta^2 z^{2/3} / \theta_*^2$ as a function of stability under different conditions. These results are in agreement with Davidson *et al.* (1978).

Model Results

Several results of the model are presented graphically. In these figures, the solid curves in the figures are from model calculations based on C_{DN} whereas the dashed curves are from model calculations based on z_{ou} (Charnock's equation). If not mentioned explicitly, the relative humidity is set to 80 % and the sea surface temperature is set to 10 °C (note that the ASTD is the driving parameter and not the sea surface temperature). The relative humidity of the air just above the sea surface is 98 %. The following exchange coefficients were selected: neutral drag coefficient of $C_{DN} = (0.58 + 0.085 U_{10N}) 10^{-3}$, Stanton number $C_{HN} = 1.0^{-3}$ and Dalton number $C_{EN} = 1.2 10^{-3}$.

Stability at the standard height of 10 m

One of the essential parameters in micrometeorology is the atmospheric stability parameter ζ , defined as z/L , the ratio of the height z and the Monin-Obukhov length L . In the marine surface layer the stability parameter is mainly controlled by the wind speed and the Air-Sea Temperature Difference, abbreviated by ASTD. (The relative humidity has a minor influence on the stability term.) Positive values of ζ indicate a stable atmosphere in which turbulent mechanical mixing is inhibited by positive temperature gradients (cold eddies cannot rise to higher and warmer levels). This situation is also called a stratified atmosphere, see e.g. Panofski and Dutton (1984) and Smith (1988). Negative values of the stability parameter indicate an unstable atmosphere where turbulent mechanical mixing is enhanced or even dominated by convective processes. In (near) neutral conditions, mechanical mixing dominates. Figure 2.2 shows a plot of the stability parameter as function of the ASTD and the wind speed at 10 m altitude (not the neutral wind speed).

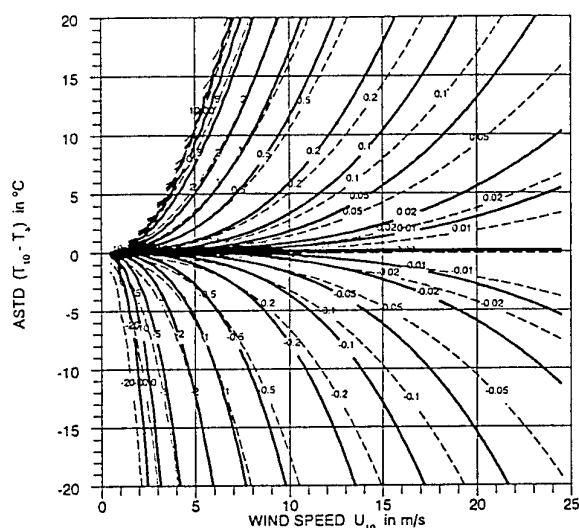


Fig. 2.2: Stability as a function of wind speed and air-sea temperature difference (ASTD) both at the standard height of 10 m. The solid curves are from the model based on C_{DN} and the dashed curves are from the model based on z_{0w} .

The curves in this figure can be used to quickly estimate the stability parameter from standard meteorological observations. The strong non-linear relation between the meteorological condition and the stability parameter becomes evident from this figure. For a given ASTD, the absolute value of the stability parameter decreases with increasing wind speed (mechanical mixing becomes more important) whereas for a given wind speed, the stability parameter increases with increasing ASTD (convective processes become important). It is estimated from the results in Figure 2.2 that the results of the two models agree within about 20 %. Calculations with a relative humidity of 95 % provide a set of curves which are almost similar to those presented in Figure 2.2.

Friction velocity and roughness length for wind speed

To estimate the controlling parameters for calculating the vertical profile of wind speed and the momentum flux, plots of the friction velocity u_* and the roughness length z_{ou} as a function of the actual wind speed at 10 m altitude (not the neutral wind speed at 10 m) and the 10 m value of the ASTD are presented in Figure 2.3a+b. Note that the differences between the friction velocities predicted by the two models increases with wind speed but remains within about 10 %. On the other hand, the differences between the roughness lengths of the two models can be as large as a factor 3.

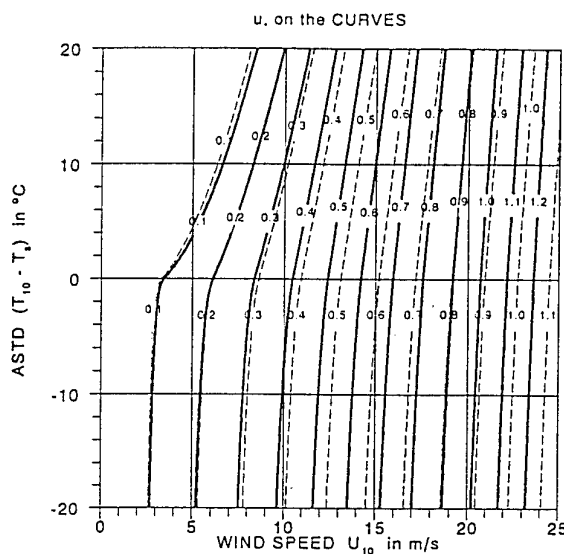


Fig. 2.3a: Friction velocity as a function of wind speed and air-sea temperature difference (ASTD) both at the standard height of 10 m. The solid curves are from the model based on C_{DN} and the dashed curves are from the model based on z_{ou} .

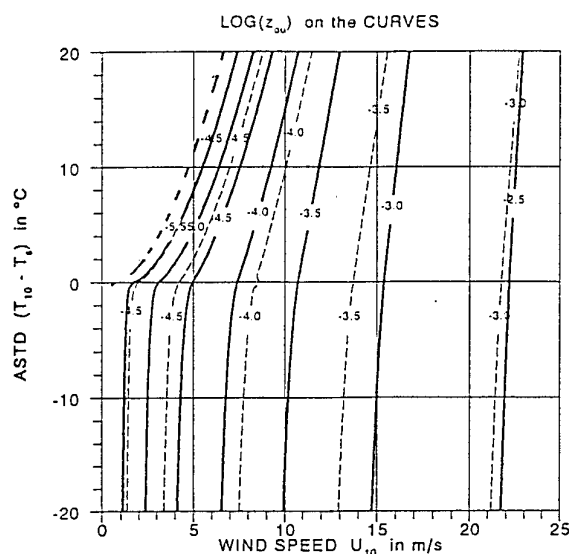


Fig. 2.3b: Roughness length for wind speed as a function of wind speed and air-sea temperature difference (ASTD) both at the standard height of 10 m. The solid curves are from the model based on C_{DN} and the dashed curves are from the model based on z_{ou} .

Vertical profiles of wind speed

The vertical profiles of wind speed, in turn, are calculated from the roughness length for wind speed, the friction velocity and the stability parameter, i.e. equation (2.15). The results of these calculations for different values of the ASTD (thus different stabilities) and for a fixed wind speed of 10 m/s at 10 m height, are shown in Figure 2.4. Note that under unstable conditions (sea warmer than the air, convective processes become dominant) the vertical profiles of the wind speed are all alike whereas under stable conditions (stratified atmosphere), the variation of the wind speed with altitude is very strong. Note also that the differences between the two models is no more than 3 % although the individual differences of the roughness lengths and the friction velocity between the two models was larger.

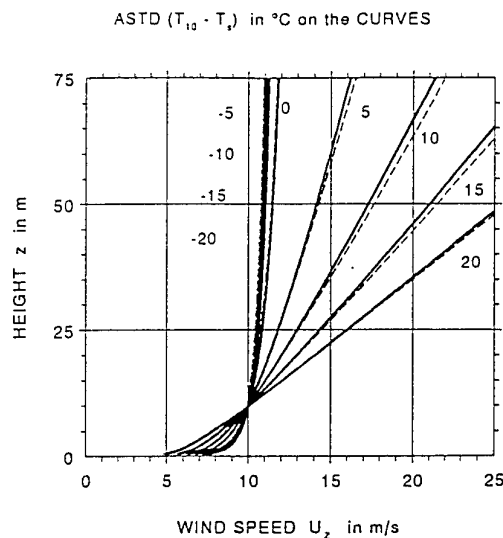


Fig. 2.4: Vertical profiles of wind speed for different values of the air-sea temperature difference (ASTD) at the standard height of 10 m. The solid curves are from the model based on C_{DN} and the dashed curves are from the model based on z_{0w} .

Apparently, the profiles of the wind speed (within the plotted interval) are less sensitive to variations in these parameters. An analytical sensitivity analysis would be necessary to describe exactly the influence these parameters, but the complex relation of the equations makes this very difficult if ever possible. Nevertheless, a short analytical sensitivity study has been carried out for special conditions as shown in Appendix C.

Scaling temperature and roughness length for temperature

Figure 2.5a+b show the the scaling (potential) temperature and the roughness length for temperature as a function of the 10 m values of the ASTD and the wind speed (not neutral wind speed). Apart from the stability parameter which is shown in Figure 2.2, these parameters controll the vertical profile of the ASTD.

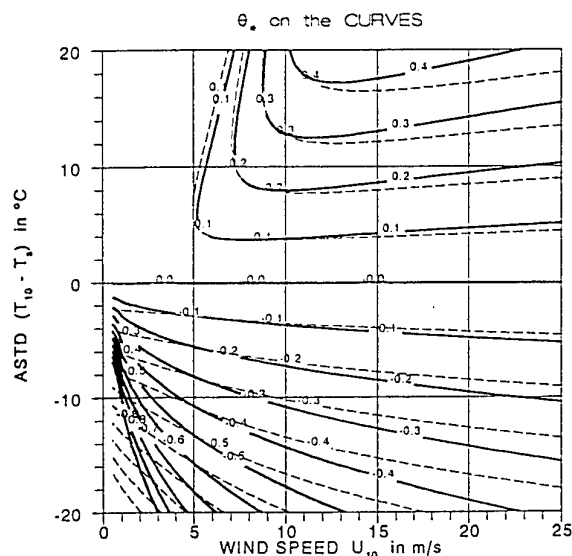


Fig. 2.5a: Potential scaling temperature as a function of wind speed and air-sea temperature difference (ASTD) both at the standard height of 10 m. The solid curves are from the model based on C_{DN} and the dashed curves are from the model based on z_{ow} .

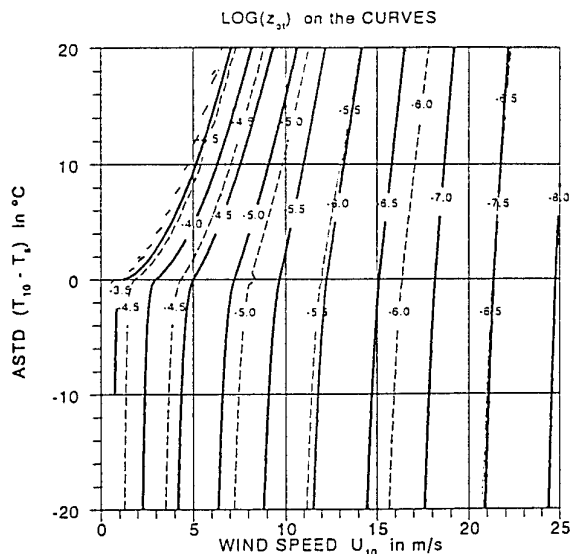


Fig. 2.5b: Roughness length for temperature as a function of wind speed and air-sea temperature difference (ASTD) both at the standard height of 10 m. The solid curves are from the model based on C_{DN} and the dashed curves are from the model based on z_{our} .

Note that the differences between the two models are small for the scaling temperature (Figure 2.5a) but can become as large as about a factor 10 for the temperature roughness length. The lack of lines for positive ASTD values and low wind speeds in Figure 2.5a indicate the region of very stable conditions with very limited exchange of heat between atmosphere and sea. At higher wind speeds, however, mechanical turbulence helps to exchange heat. Note that for positive values of the ASTD the scaling temperature varies sharply with wind speed in the interval between 5 to 10 m/s.

Vertical temperature profiles

Vertical temperature profiles are calculated using equation 2.16 and the data shown Figure 2.2 and Figure 2.5a+b for the stability, the scaling temperature and the temperature roughness length. Some of these temperature profiles for different wind speeds are shown in Figure 2.6. Note that for negative values of the ASTD (unstable condition), the gradients in the temperature are very strong due to vertical turbulent mixing and that the shapes of the temperature profiles do not differ much (temperature becomes almost independent with height) except for about the lowest 5 to 10 m. Under stable conditions (positive ASTD; stratified atmosphere), on the other hand, the shapes of the temperature profiles differ much and the variation with height is stronger due to a lack of vertical turbulent mixing.

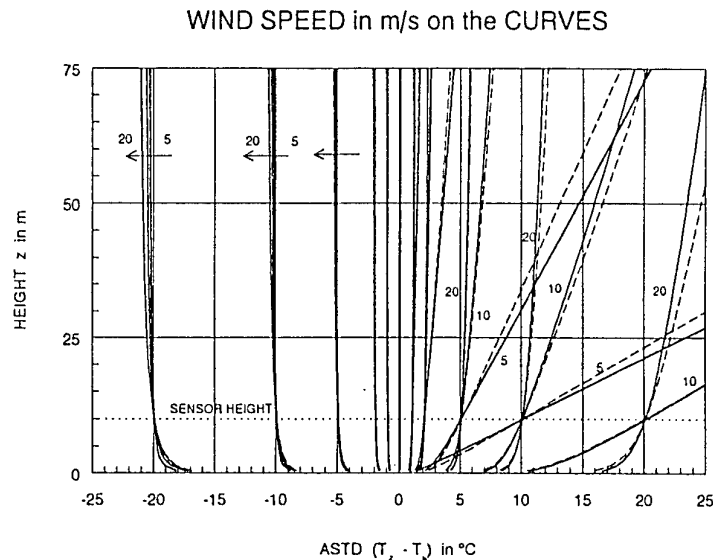


Fig. 2.6: Vertical profiles of the air-sea temperature difference (corrected for height) for different values of the wind speed at the standard height of 10 m. The solid curves are from the model based on C_{DN} and the dashed curves are from the model based on z_{0u} .

Scaling specific humidity and roughness length for humidity

The variation of the scaling humidity and the roughness length for humidity under different meteorological conditions are presented in Figure 2.7a+b. Vertical profiles of specific humidity difference under several conditions have been presented in Figure 2.8. Because the specific humidity is described with a set of equations that is analogue to the temperature, the figures of humidity and temperature have much in common.

Fluxes of momentum, heat and water vapor

The developed models can also provide the fluxes of momentum, heat and water vapor. However, these fluxes are less relevant to describe optical turbulence. Therefore, some of these calculations are shifted towards Appendix D, where the fluxes are presented as a function of wind speed and ASTD.

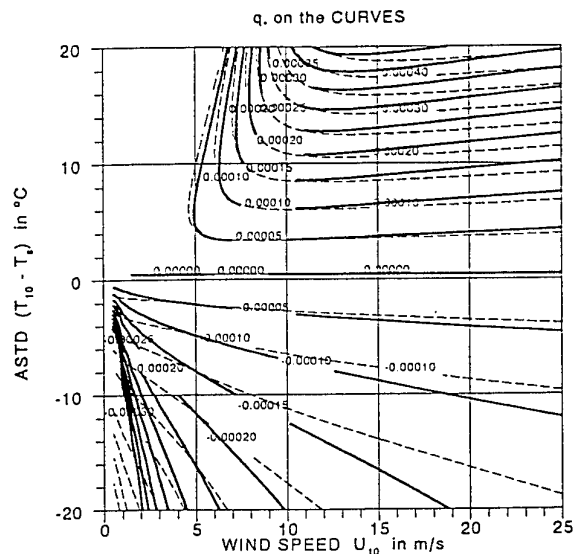


Fig. 2.7a: Scaling humidity as a function of wind speed and air-sea temperature difference (ASTD) both at the standard height of 10 m. The solid curves are from the model based on C_{DN} and the dashed curves are from the model based on z_{0w} .

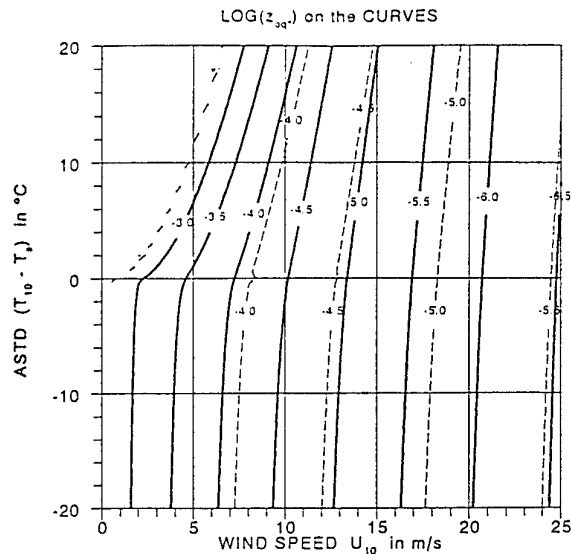


Fig. 2.7b: Roughness length for humidity as a function of wind speed and air-sea temperature difference (ASTD) both at the standard height of 10 m. The solid curves are from the model based on C_{DN} and the dashed curves are from the model based on z_{0w} .

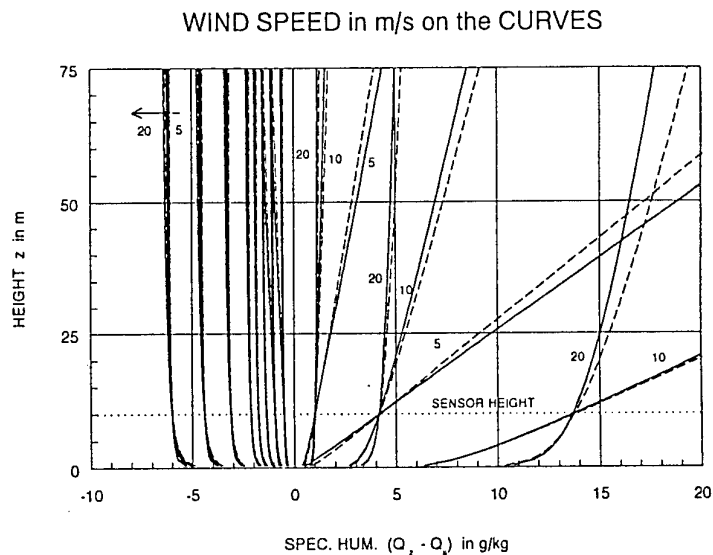


Fig. 2.8: Vertical profiles of the air-sea specific humidity difference for different values of the wind speed at the standard height of 10 m. The solid curves are from the model based on C_{DN} and the dashed curves are from the model based on z_{0w} .

Summary

A method is presented to estimate the vertical turbulent fluxes of momentum, sensible heat and water vapor in the marine surface layer from wind speed, air temperature, air humidity and sea surface temperature and the height at which these data were measured. In addition, the method uses the 10 m neutral exchange coefficients (drag coefficient, Stanton and Dalton number). The results compare favourably with those found in literature. The vertical profiles of wind speed, temperature and humidity in the marine surface layer can be calculated from the scaling parameters and the roughness lengths which are also provided by the model. The vertical profiles of temperature and humidity provide basic information for the calculation of the vertical profiles of the refractive index to predict refractivity effects, whereas the scaling parameters are required to predict effects of optical turbulence.

3. Optical parameters

3.1 Introduction

The refractive index of air, as function of wavelength, can be derived from the gas-composition, air pressure and air temperature, see e.g. Edlén (1953, 1966), Owens (1967) and Friehe *et al.* (1975). Thus, using the vertical profiles of air temperature, air pressure and water vapor, which can be predicted using the micrometeorological model as discussed in the previous section, the vertical profiles of the refractive index can be calculated. As a result, effects such as sub- and super refraction, ducting and image distortion can be predicted on the basis of standard meteorological observations only. However, due to atmospheric turbulence, both the air temperature and air humidity fluctuate around a mean value (both in time and in space) resulting in a fluctuating refractive index. Consequently, the 'rays' from a target are slightly bended in an irregular fashion around the mean direction, which results in effects such as scintillation, blurring and image dancing. Because (optical) turbulence can only be described statistically, it is not possible to predict either the spatial and/or the temporal behaviour. This problem becomes even more complex because these effects are a non linear function of height, range and the micrometeorological parameters. Moreover, scintillation seems to saturate.

A derivation of the equations that describe optical/infrared turbulence is a theoretical task which is beyond the scope of this work. Therefore, only the results will be presented here that are found in many publications and standard books such as Hufnagel (1978) and Beland (1993).

In this section equations are presented that have been applied in our model to predict optical refractivity effects and optical turbulence in the marine surface layer. These effects are expressed in terms of micrometeorological parameters such as described in Chapter 2. The performance of some aspects of the model are verified against data available from literature. Some results from the model are presented in graphical form.

3.2 Refractive index of air

The refractive index of air varies with wavelength and is a function of gas composition and air pressure. In the present model, we confine ourselves to relatively simple models for the refractive index of air such as from Edlén (1966), Owens (1967) and Friehe *et al.* (1975). In these models, the refractive index of air varies relatively slowly with wavelength and effects due to molecular absorption are ignored. It was found (Kunz, 1993) that the agreement of these models, as regards the variation of the refractivity with temperature, humidity and pressure, was better than 97 %. For the present model, the equation for the refractivity of

Edlén was chosen because it is applicable from 0.23 μm to the infrared (Fenn *et al.*, 1985; an alternate expression can be found in Thomas and Duncan, 1993).

The refractivity according to Edlén is given by:

$$N = \left[a_0 + \frac{a_1}{1 - (\nu / b_1)^2} + \frac{a_2}{1 - (\nu / b_2)^2} \right] \frac{P}{P_o} \frac{(T_o + 15.0)}{T} - [c_0 - (\nu / c_1)^2] \frac{P_w}{P_o} \quad (3.1)$$

where:

- a_0 = 83.42;
- a_1 = 185.08;
- a_2 = 4.11;
- b_1 = $1.140 \cdot 10^5$;
- b_2 = $6.24 \cdot 10^4$;
- c_0 = 43.49;
- c_1 = 43.49;
- c_2 = $1.7 \cdot 10^4$;
- N = $(n-1) \cdot 10^6$ is refractivity with n the refractive index;
- P = total air pressure in hPa;
- P_o = reference pressure of 1013.35 hPa;
- P_w = water vapor pressure in hPa;
- T = air temperature in K;
- T_o = reference temperature, 273.15 K;
- ν = $10^4 / \lambda$; ν is frequency in cm^{-1} and λ is wavelength in μm .

Dependence of the refractivity on temperature and relative humidity

To get some insight in the dependence of the refractivity on commonly measured atmospheric parameters, equation (3.1) has been used to calculate the refractivity for two optical wavelengths (0.55 μm and 10.0 μm) over an air temperature interval from -10 to +30 $^{\circ}\text{C}$ and a relative humidity interval from 20 to 100 %. The results are presented in Figure 3.1. (The graph in Appendix E can be helpful to convert combinations of temperature and relative humidity to the specific humidity.) The solid lines represent the refractivity ($10^{-6} N = n - 1$) for 0.55 μm and the overlapping dashed lines are for 10.0 μm . Most important is to realize that over the interval of interest the refractivity varies relatively strong with air temperature but only slightly with relative humidity. In addition, note that there is a strong similarity between the variations of the refractivity with temperature and/or relative humidity for both wavelengths. This means that the refractive index structure function parameter C_n^2 , such as described in equation (3.7), for the two wavelengths are very much alike.

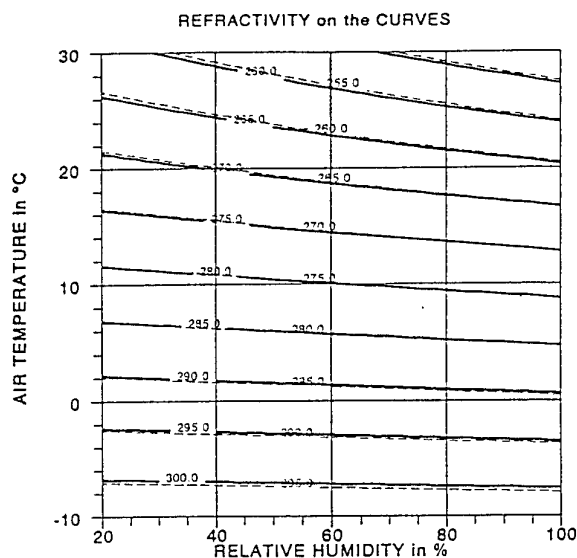


Fig. 3.1: Refractivity as a function of air temperature and relative humidity. The solid lines are for a wavelength of $10\ \mu\text{m}$ and the dashed lines are for $0.55\ \mu\text{m}$.

Refractivity profiles

Refraction effects in a horizontally stratified atmosphere are controlled by the vertical profile of the refractive index, and thus by the profiles of air temperature, humidity and pressure. Using meteorological observations in combination with the micrometeorological model described in the previous section, the vertical profiles of the refractivity can be calculated. In Figure 3.2 results of such calculations are presented, for three different conditions, with the air temperature higher, equal or lower than the sea surface temperature, under the condition $T_{\text{sea}} = 10\ ^\circ\text{C}$, $\text{RH} = 80\%$, $U_{10} = 10\ \text{m/s}$, $P = 1025\ \text{hPa}$. The solid lines represent the refractivity at $0.55\ \mu\text{m}$ and the dashed lines are for $10\ \mu\text{m}$. The curves for $T_a = 10\ ^\circ\text{C}$ show a decreasing refractivity with height due to the negative pressure gradient which can lead to super refractivity effects (Thomas and Duncan, 1993).

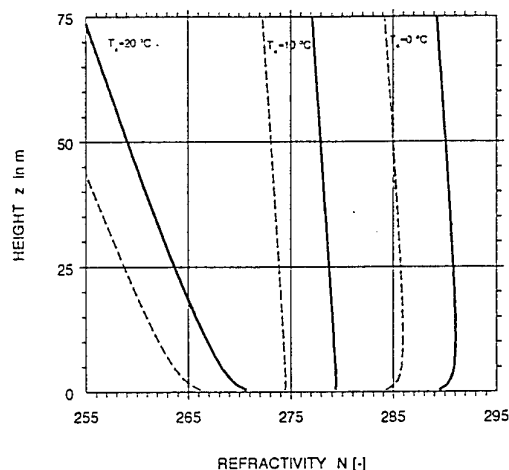


Fig. 3.2: Vertical profiles of the refractivity for three different air temperatures. The solid lines are for a wavelength of $10\ \mu\text{m}$ and the dashed lines are for $0.55\ \mu\text{m}$. Other parameters: $T_{\text{sea}} = 10\ ^\circ\text{C}$, $\text{RH} = 80\%$, $U_{10} = 10\ \text{m/s}$, $P = 1025\ \text{hPa}$.

When the air temperature is higher than the sea surface temperature (stable situation; most left curves in Figure 3.2) the air density and thus the refractivity decreases stronger with height which can also result in super refractivity effects. When the sea surface temperature is higher than the air temperature (unstable situations), the refractivity near the sea surface is lower and will increase gradually with height (due to the colder air temperature). Observations in such a layers can be effected by sub refractivity. Of course, for larger heights, the refractivity decreases again due to the negative pressure gradient resulting in a duct of the refractive index.

3.3 Optical turbulence

Optical turbulence is caused by variations of the refractive index due to complex spatial and temporal atmospheric variations. The variations are caused by wind shear and/or by convective process due to vertical gradients in wind speed, temperature and humidity. Therefore, optical and infrared turbulence are closely related to atmospheric turbulence. In accordance with other turbulent quantities, optical turbulence is expressed in the structure function, $D_{nn}(R)$, which is defined as the ensemble average of the refractive index difference $\langle (n_{R_2} - n_{R_1})^2 \rangle$ between two points of observation $R = R_2 - R_1$. Mathematically the structure function is written as:

$$D_{nn}(R) = \langle (n_{R_2} - n_{R_1})^2 \rangle = \langle (dn)^2 \rangle \quad (3.2)$$

Dimensional analysis can prove that the relation between the structure function and the distance between the points of observations are related to the structure function parameter for the refractive index C_n^2 . According to the notation of, e.g., Beland (1993) we write:

$$D_{nn}(R) = C_n^2 R^{2/3} \quad (3.3a)$$

Sometimes it can be helpful to describe the structure function $D_{nn}(R)$ in terms of the total variance of the refractive index σ_n^2 and in the spatial autocorrelation function $\rho_n(R)$ of the refractive index. By rewriting equation (3.2) in terms of the mean and the variation of the refractive index it can easily be shown that:

$$D_{nn}(R) = 2 \sigma_n^2 [1 - \rho_n(R)] \quad (3.3b)$$

In order to relate the (micro)meteorological turbulence to the optical turbulence, the variation of the refractive index is rewritten in the variations of air temperature, air humidity and air pressure as shown in equation (3.4):

$$dn = \frac{\partial n}{\partial T} dT + \frac{\partial n}{\partial q} dq + \frac{\partial n}{\partial P} dP \quad (3.4)$$

Because pressure variations in atmospheric eddies are small and have only a slight influence on the refractive index variation, the last term in equation (3.4) can be ignored. Substitution of the square of the variation of the refractive index in equation (3.2) results in:

$$D_{nn}(R) = \left\langle \left(\frac{\partial n}{\partial T} dT \right)^2 + \left(\frac{\partial n}{\partial q} dq \right)^2 + 2 \left(\frac{\partial n}{\partial T} \frac{\partial n}{\partial q} dT dq \right) \right\rangle \quad (3.5)$$

The last term in this equation describes the eddy covariance between the temperature and the humidity. Rewriting of equation (3.5) in terms of structure functions results in:

$$D_{nn}(R) = \left(\frac{\partial n}{\partial T} \right)^2 D_{TT}(R) + \left(\frac{\partial n}{\partial q} \right)^2 D_{qq}(R) + 2 \left(\frac{\partial n}{\partial T} \frac{\partial n}{\partial q} \right) D_{Tq}(R) \quad (3.6)$$

Substitution of the structure function constants for refractive index, temperature, humidity and the covariance between temperature and humidity results in:

$$C_n^2 = \left(\frac{\partial n}{\partial T} \right)^2 C_T^2 + \left(\frac{\partial n}{\partial q} \right)^2 C_q^2 + 2 \left(\frac{\partial n}{\partial T} \frac{\partial n}{\partial q} \right) C_{Tq} \quad (3.7)$$

This very important equation describes the relation between atmospheric turbulence on one side and the optical/infrared turbulence on the other side. The dependence of the refractive index on temperature and humidity are known from Edlén's work and the structure function constants for temperature and humidity can either be measured or estimated from the scaling temperature and the scaling humidity, the stability and the height -equations (2.36) to (2.38)- using the bulk model described in the previous chapter.

Approximation of small variations of the refractive index

The structure function parameter for the refractive index is related to optical effects caused by turbulence (such as scintillation and blurring) using the Rytov approximation. In this approach it is assumed that the dimensions of the refractive index variations are large compared to the dimensions of the electromagnetic field (e.g. Hufnagel 1964, Lawrence 1970, Hufnagel, 1978 and Beland, 1993).

The Rytov approximation assumes that the variations of the real and the imaginary component of the propagation constant, respectively χ and ϕ , are Gaussian distributed with zero mean and standard deviations σ_χ and σ_ϕ . If no energy is lost over the path of observation, the real part of the variable refractive index describes the fluctuation of the signal (scintillation) whereas the imaginary part distorts the phase of the wavefront, resulting in effects such as blurring and image dancing. Because the variations in χ and ϕ are normally distributed, the fluctuations in intensity and deformation are log normally distributed.

Structure function parameters versus wind speed and ASTD

The structure function parameter for the refractive index is the driving factor for the description of optical turbulence effects. C_n^2 has been calculated for wind speeds from 0 to 25 m/s and ASTD from -20 to +20 °C, both taken at the standard height of 10 m. The results are presented in Figure 3.3a+b as contour lines of (the 10-based logarithm of) equal refractive index structure function parameter. The solid and the dashed lines are respectively from the model driven by C_{DN} and z_{ou} . Although the refractive index of air is a function of wavelength, the variation of the refractive index with temperature and humidity is less dependent on wavelength as can be seen from Figure 3.1. Consequently, the results for 0.55 μm and for 10 μm wavelength are very similar as shown in Figure 3.3a+b.

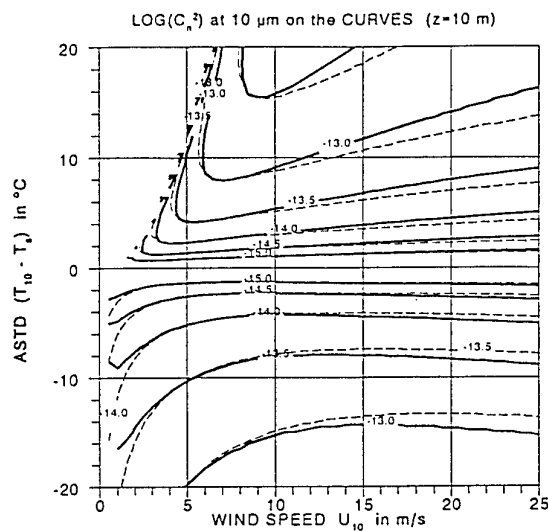


Fig. 3.3a: Refractive index structure function parameter at a wavelength of 10 μm as a function of wind speed and air-sea temperature difference (ASTD) both at the standard height of 10 m. The solid curves are from the model based on C_{DN} and the dashed curves are from the model based on z_{ou} .

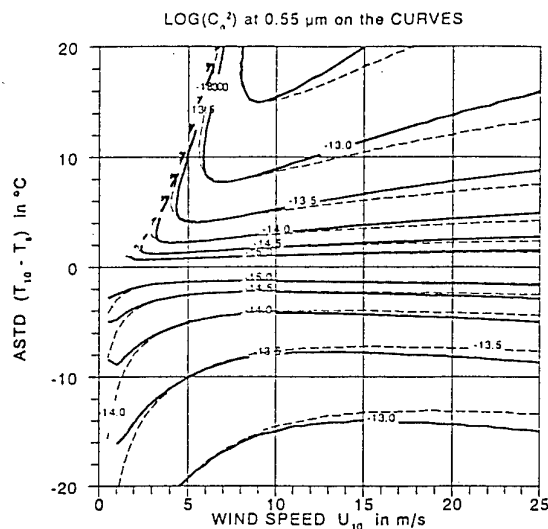


Fig. 3.3b: Refractive index structure function parameter at a wavelength of 0.55 μm as a function of wind speed and air-sea temperature difference (ASTD) both at the standard height of 10 m. The solid curves are from the model based on C_{DN} and the dashed curves are from the model based on z_{ou} .

Under stable conditions (positive ASTD) and low wind speeds, the refractive index structure function parameter has a very low value. Initially, the value of C_n^2 increases sharply with wind speed followed by a slowly decrease. The region in which the curves are parallel or almost parallel with the horizontal axis, indicate the conditions where the refractive index structure function parameter is independent of wind speed.

The explicit dependence of the refractive index structure function parameter on wind speed and on ASTD is shown in Figure 3.4a+b, respectively with the ASTD and the wind speed as parameter. The sharp gradient in C_n^2 as a function of wind

speed for positive ASTD values is clearly visible in Figure 3.4a for relatively low wind speeds. At higher wind speeds, the values of C_n^2 decrease slowly and it seems that C_n^2 becomes independent of the sign of the ASTD. The asymmetry in Figure 3.4b indicates that the variation of C_n^2 with ASTD is stronger for positive values of the ASTD than for the negative values of the ASTD. Note also that for low but fixed wind speeds there is a maximum in C_n^2 . This is caused by the damping of mechanical turbulence in stratified situations.

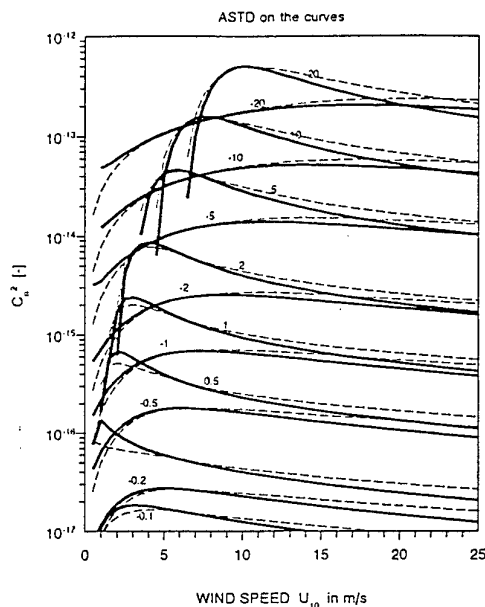


Fig. 3.4a: Refractive index structure function parameter for $0.55 \mu\text{m}$ and for $10 \mu\text{m}$ as a function of the wind speed at the standard height of 10 m. ASTD is on the curves. The solid curves are from the model based on C_{DN} and the dashed curves are from the model based on z_{ou} .

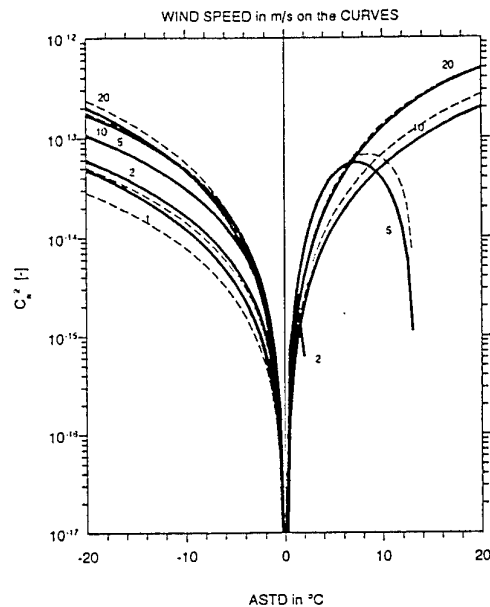


Fig. 3.4b: Refractive index structure function parameter for $0.55 \mu\text{m}$ and $10 \mu\text{m}$ as a function of the air-sea temperature difference (ASTD) at the standard height of 10 m. Wind speed is on the curves. The solid curves are from the model C_{DN} and the dashed curves are from the model based on z_{ou} .

Vertical profiles of the refractive index structure function parameter

Because both the structure function parameters for temperature and for humidity (but also the covariance function) depend on height in a complex way, cf. equations (2.36) to (2.42), also the structure function parameter for the refractive index varies with height. This is illustrated in Figure 3.5 for different values of the ASTD and for a fixed value of the wind speed of 10 m/s. The results from the model based on C_{DN} and based on z_{ou} are respectively presented by the solid lines and by dashed lines. The strong negative gradients in the refractive index structure function parameter at low elevation, typically below 10 m, are apparent. As a result, we may expect that the strongest contribution of turbulence comes from the lowest altitudes under all conditions. During unstable (well mixed) conditions and for heights above 10 m, the refractive index structure function parameter decreases only slightly with height whereas under stable conditions, the refractive index structure function parameter decreases strongly with height.

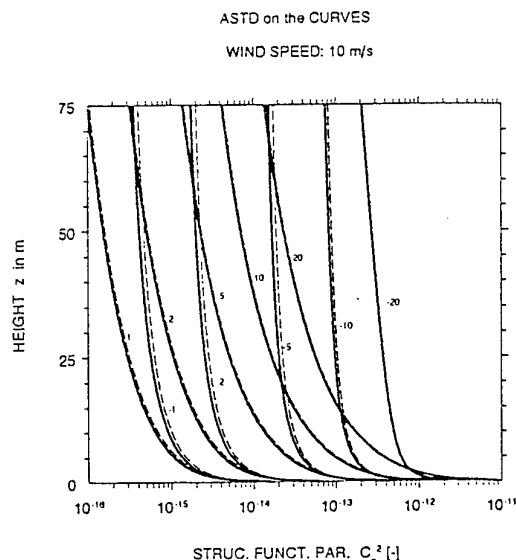


Fig. 3.5: Vertical profiles of the structure function parameter for the refractive index for $10\ \mu\text{m}$ and for $0.55\ \mu\text{m}$ at a wind speed of $10\ \text{m/s}$. The air-sea temperature difference (ASTD) is on the curves. The solid curves are from the model based on C_{DN} and the dashed curves are from the model based on z_{0w} .

3.4 Scintillation

Scintillation is assumed to be caused by the randomly variable, normally distributed, real part of the propagation constant, σ_χ . The Rytov approximation predicts the following relation between σ_χ and the structure function parameter for the refractive index C_n^2 over a non homogeneous path R . See, e.g., Andreas (1988), Beland (1988, 1993) and Ochs and Wang (1978).

$$\sigma_\chi^2(R) = 0.56 \left(\frac{2\pi}{\lambda} \right)^{7/6} \int_0^R C_n^2(r) \left(\frac{r}{R} \right)^{5/6} (R-r)^{5/6} dr \quad (3.8a)$$

where :

- λ = wavelength in μm ;
- C_n^2 = refractive index structure function parameter in $\text{m}^{-2/3}$;
- R = range in m;
- r = integration variable in m.

In the case of isotropic turbulence (see e.g. Hill and Ochs 1978, Wang and Ochs 1978), equation (3.8) reduces to:

$$\sigma_\chi^2(R) = 0.124 C_n^2 \left(\frac{2\pi}{\lambda} \right)^{7/6} R^{11/6} \quad (3.8b)$$

However, because Rytov's approximation is based on weak turbulence only (see e.g. Hufnagel, 1978 and Beland, 1993) the equations (3.8a+b) do not predict the saturation of σ_χ^2 at a value of about 0.3 ($\sigma_\chi > 0.55$) which is observed experimentally.

Scintillation is described in terms of a Gaussian distributed electromagnetic propagation constant with standard deviation σ_χ . As a result, the intensity variations are log-normally distributed. Using the property of the log-normal distribution which relates the mean intensity and the standard deviation, see, e.g., Hufnagel (1978), Goodman (1985) and Beland (1993), we can write:

$$\frac{\sigma_I^2}{\bar{I}^2} = e^{4\sigma_\chi^2} - 1 \quad (3.9)$$

Due to the saturation effect, the ratio of the standard deviation and the mean intensity saturates at about 1.1 (see e.g. Beland 1993).

The scintillation expressed as the ratio between the standard deviation and the mean intensity, has been calculated with the micrometeorological model in combination with the above mentioned equations for a number of different meteorological conditions, for two optical wavelengths and for two ranges. Isotropic turbulence is assumed. The results of these calculations are presented in Figure 3.6a+b+c+d as a function of ASTD and wind speed. The white areas represent conditions where scintillation saturation occurs. Note that under weak turbulent conditions, systems operating in the infrared are less sensitive to turbulence than systems operating in the visible due to the wavelength dependence as shown in equation (3.8). However, under conditions of strong turbulence when scintillation saturation occurs, there is no preference for a certain system. The parallelism of the contour lines with the horizontal axis in the figure indicate that the scintillation is mainly ASTD driven and not by the wind. This is in accordance with the other contour plots.

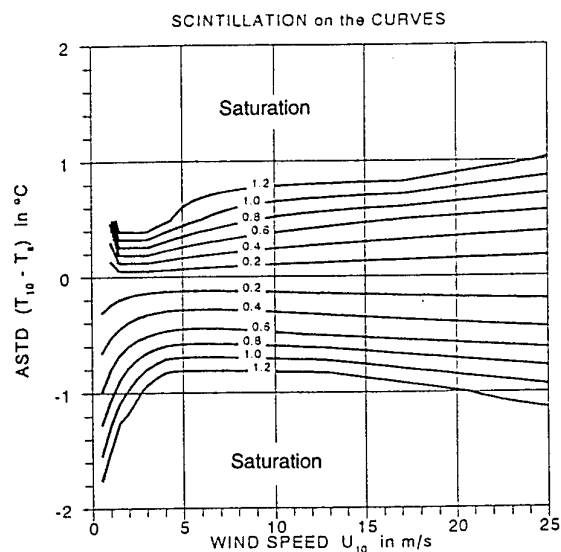


Fig. 3.6a: Scintillation at a wavelength of $0.55 \mu\text{m}$ over a 10 km path as a function of wind speed and air-sea temperature difference (ASTD) both at the standard height of 10 m.

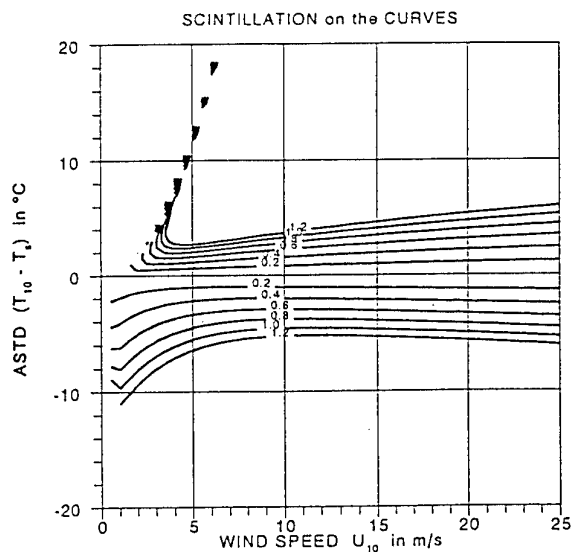


Fig. 3.6b: Scintillation at a wavelength of $10 \mu\text{m}$ over a 10 km path as a function of wind speed and air-sea temperature difference (ASTD) both at the standard height of 10 m.

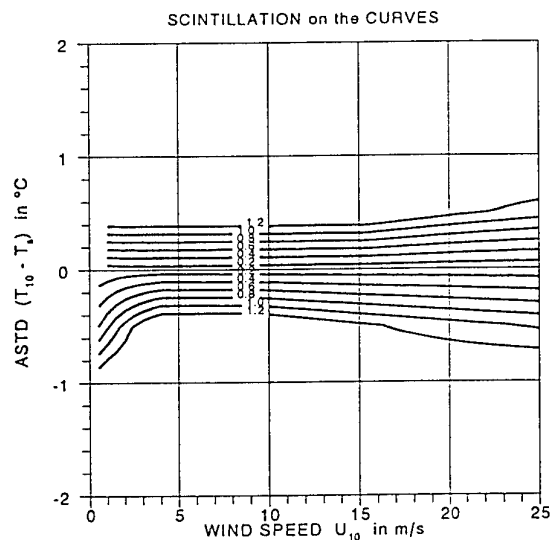


Fig. 3.6c: Scintillation at a wavelength of $0.55 \mu\text{m}$ over a 20 km path as a function of wind speed and air-sea temperature difference (ASTD) both at the standard height of 10 m.

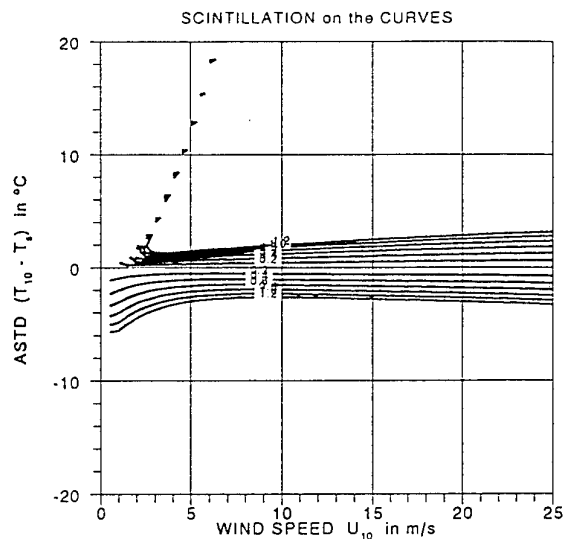


Fig. 3.6d: Scintillation at a wavelength of $10 \mu\text{m}$ over a 20 km path as a function of wind speed and air-sea temperature difference (ASTD) both at the standard height of 10 m.

3.5 Blurring

For the description of blur, image dancing and deformation, the transversal coherence length ρ_o is used as the controlling parameter. This parameter describes the transversal coherence length of an ideal plane wave after having travelled over a certain path length through the atmosphere. According to Beland (1993) it is defined as:

$$\rho_o = \left[1.46 \left(\frac{2\pi}{\lambda} \right)^2 \int_0^R C_n^2(r) (r/R)^{5/3} dr \right]^{-3/5} \quad (3.10a)$$

which for isotropic turbulence reduces to:

$$\rho_o = \left[0.55 \left(\frac{2\pi}{\lambda} \right)^2 C_n^2 R \right]^{-3/5} \quad (3.10b)$$

Before proceeding, the atmospheric coherence length r_o is introduced. r_o is directly derived from the transversal coherence length ρ_o according to:

$$r_o = 2.1 \rho_o \quad (3.11)$$

The atmospheric coherence length can be regarded as the maximum diameter of the optics before the effect of turbulence distorts the image.

The atmospheric modulation transfer function is derived using the transversal coherence length. Beland's equation for the MTF, expressed in cycles per unit length for a system with focal length f , for long term exposure is:

$$MTF(v) = \exp[-3.44 (\lambda f v / r_o)^{5/3}] \quad (3.12a)$$

and for short term exposure:

$$MTF(v) = \exp\left[-3.44 (\lambda f v / r_o)^{5/3} \{1 - b(\lambda f v / D)^{1/3}\}\right] \quad (3.12b)$$

For our (far field) applications, the constant b in the equation is taken to be 0.5 (Beland, 1993). Equation (3.12b) shows that for short term exposure, the atmospheric turbulence cannot be treated independently from the system.

The blur size has been approximated by considering that one line pair in the focal plane can be represented by an angle of $1/fv$ (radians) and that the influence of turbulence becomes only noticeable under conditions where r_o becomes so small that the numerical value of the exponent in equation (3.12a+b) reduces to -1. The discussion about this definition of the blur size is beyond the scope of this work. We have calculated the angle of a single line pair for different meteorological

conditions, for two optical wavelengths and two ranges. The results of the calculations are presented as contour lines of equal blur size in Figure 3.7a+b+c+d. It is noted from the figures that the blur in the IR is about a factor of two smaller than in the visible. In addition, the figures show again the strong influence of the ASTD on the blur size and the weak influence of the wind speed.

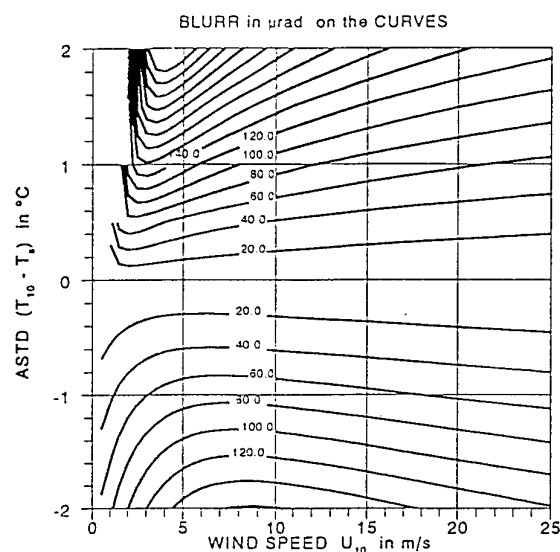


Fig. 3.7a: Blur in μrad at a wavelength of $0.55 \mu\text{m}$ over a 10 km path as a function of wind speed and air-sea temperature difference (ASTD) both at the standard height of 10 m.

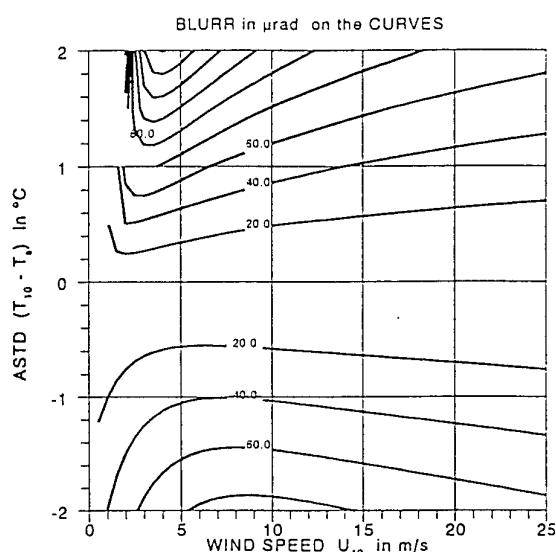


Fig. 3.7b: Blur in μrad at a wavelength of $10 \mu\text{m}$ over a 10 km path as a function of wind speed and air-sea temperature difference (ASTD) both at the standard height of 10 m.

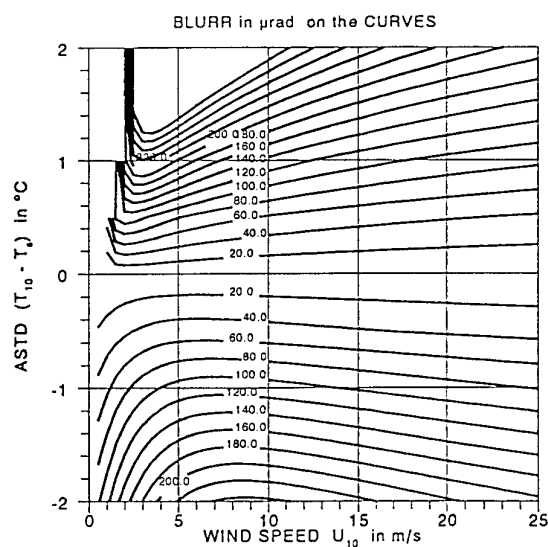


Fig. 3.7c: Blur in μrad at a wavelength of $0.55 \mu\text{m}$ over a 20 km path as a function of wind speed and air-sea temperature difference (ASTD) both at the standard height of 10 m.

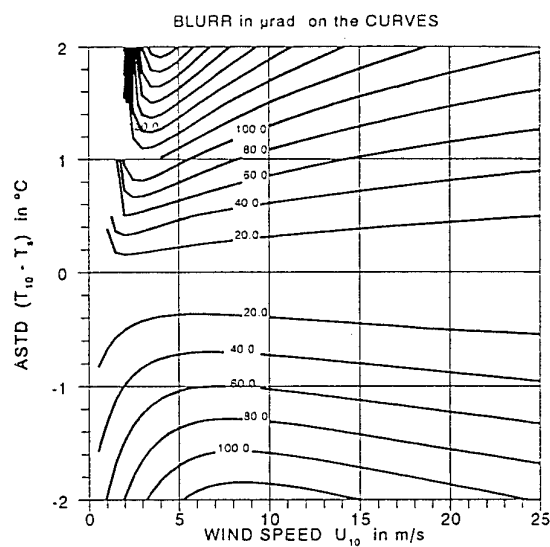


Fig. 3.7d: Blur in μrad at a wavelength of $10 \mu\text{m}$ over a 20 km path as a function of wind speed and air-sea temperature difference (ASTD) both at the standard height of 10 m.

3.6 Image motion

Image motion is expressed as the variation around a mean value of the angle of arrival of a plane wave. Hufnagel (1978) shows that the variance of the angle of arrival can be expressed as:

$$\langle \alpha_x^2 \rangle = \langle \alpha_y^2 \rangle \equiv 4.5 F^2 a^{-1/3} \int_0^R C_n^2(r) dr \quad (3.13)$$

where

F = focal length of the optics in m;

a = radius of the optics in m.

Although image motion cannot be decoupled from the system parameters, we can make an estimate of the angles of arrival under isotropic turbulence from the data e.g. from Figure 3.3+3.4. For a system with a focal length of 1 m, an aperture diameter of 0.2 m and a target at a distance of 10 km, the angle of arrival becomes about 77,000 times the refractive index structure function parameter. Thus for weak turbulence with $C_n^2 = 10^{-17}$, the angle of arrival becomes about 10^{-12} radians and for strong turbulence with $C_n^2 = 10^{-12}$, the angle of arrival becomes about 10^{-7} radians. With reference to the results presented in Figure 3.7, we conclude that image motion is within the blur circle.

4. Summary and conclusions

A model was developed to predict the vertical profiles of wind speed, temperature, and humidity as well as the turbulent fluxes of momentum, heat and water vapor in the marine surface layer. In addition, the model provides the vertical profile of the refractive index at the wavelength of interest and the basic parameter that is used to estimate optical effects due to turbulence, C_n^2 , the refractive index structure function parameter.

Although the primary task of the model is to predict scintillation and blurring that affect the performance of long range imaging systems, the intermediate products are useful to predict refractivity effects such as ducting and super-refraction but also the parameters for a description of the micrometeorological properties of the marine surface layer.

The primary input parameters required for the model are standard meteorological observations of wind speed, air temperature, relative humidity (or any other quantity from which the humidity can be derived, e.g., dew point) and air pressure, which need not necessarily be available at the same height or at a standard height. The sea surface temperature is also required. In the background, the model uses the relative humidity of 98 % of the air just above the sea surface and the neutral exchange coefficients for momentum, heat and water vapor. Values for these coefficients are taken from literature. Alternatively the roughness length for wind speed, based on Charnock's equation, can be used instead of the neutral drag coefficient.

The most essential part of the model, the micrometeorological kernel, is solved iteratively, and has been tested with the set of input conditions from Smith (1988). The results from the model are in excellent agreement with the data published by Smith. The calculated refractive index and its variation with temperature, humidity and pressure have been compared with two other models.

Because the results are mainly dependent on a combination of the wind speed and the air-sea temperature-difference (ASTD), and only slightly on relative humidity and air pressure, many of the results have been presented in plots as a function of with wind speed and ASTD. With these graphs it is possible to get insight in the numerical values of the stability, scaling parameters, roughness lengths, fluxes, refractivity, structure function parameters, scintillation and blur under a wide variety of conditions.

It is shown that turbulence will not only occur in unstable conditions when the sea surface is warmer than the overlaying air, but can also occur during stable conditions depending on the wind speed. The strongest variation in turbulence with wind speed, for a given ASTD, occurs at wind speeds below about 7 m/s.

For higher wind speeds, the turbulence effects are mainly controlled by the ASTD and are only slightly dependent on wind speed. Under conditions of weak turbulence (e.g. $C_n^2 < 3.0E-14$), sensors that operate in the visible part of the spectrum are much more sensitive to turbulence effects (about a factor 5 to 10) than infrared systems. In situations of strong turbulence, scintillation saturation dominates for both wavelengths, but the blur in the infrared will be smaller than in the visible.

The lowest 5 to 10 m of the surface layer has the strongest contribution to turbulence.

5. Recommendations

The model presented in this report provides the parameters for a statistical description of the micrometeorology and optical turbulence in terms of means and standard deviations. For realistic simulations of turbulence distorted images, there is a strong need to implement temporal and spatial effects of scintillation and blur. This can be realized by taking into account the spectral behaviour of turbulence. In addition the model can be expanded with ray tracing capabilities to study refraction effects and/or for estimating path integrated turbulence effects.

6. Acknowledgement

The necessity of the work described in this report initiated from discussions with Stu Smith (BIO, Canada), Wiebe Oost (KNMI, The Netherlands), Wim Kohsiek (KNMI, The Netherlands) and Gerrit de Leeuw (TNO-FEL) during and after the field experiments in the autumn of 1993. Interest for optical and infrared turbulence grew as it appeared that this phenomenon could directly be coupled to bulk meteorological observations whereas the enthusiasm for this work was born during the data-analysis of the 1993 experiments, in particular after in depth discussions with Stu Smith and Ken Davidson (NPS, USA), on sabbatical leave at TNO-FEL, and from the lectures given by Prof. H. Tennekes (VU, Amsterdam, The Netherlands). I am indebted to the above mentioned persons because it is my feeling that their stimulating attitudes with respect to the subject contributed significantly to the quality of the present work. Finally, I am grateful to Arie de Jong and Kees Eberwijn for their efforts resulting in attending Tennekes' lectures.

7. References

- Anderson, R.J., and S.D. Smith, Evaporation coefficient for the sea surface from eddy flux measurements, *J. Geophys. Res.*, 86, 449-459, 1981.
- Anderson, R.J., A study of wind stress and heat flux over the open ocean by the intertial-dissipation method, *J. Phys. Oceanogr.*, 23, 2153-2161, 1993.
- Andreas, E.L., Selected papers on turbulence in a refractive medium, *SPIE Milestone Series*, vol. 25, Soc. of Photo-Optical Instrumentation Engineers, Bellingham, WA, USA, 1990.
- Beland, R.R., E.A. Murphy, G.G. Koenig, and P.C. Thomas, Comparison of horizontal scintillation measurements and models, in *Optical, Infrared and Millimeter Wave Propagation Engineering*, *SPIE Proc.* 926, 44-51, 1988.
- Beland, R.R., Propagation through Atmospheric Optical Turbulence, in *The Infrared & Electro-Optical Systems Handbook: Atmospheric Propagation of Radiation* vol. 2, edited by F.G. Smith, pp. 157-232, Infrared Information Analysis Center, Ann Arbor, Michigan 48113-4001 and SPIE Optical Engineering Press, Bellingham, WA, USA, 1993.
- Businger, J.A., Turbulent transfer in the atmospheric surface layer, in *D.A. Hagen ed., Workshop in Micrometeorology*, Boston, 1973.
- Byers, H.R., General Meteorology, McGraw Hill, 1959.
- Davidson, K.L., T.M. Houlihan, C.W. Fairall, and G.E. Schacher, Observation of temperature structure function parameter, C_T^2 over the ocean, *Bound.-Layer Meteor.*, 15, 507-523, 1978.
- Davidson, K.L., G.E. Schacher, C.W. Fairall, and A.K. Goroch, Verification of the bulk method for calculating overwater optical turbulence, *Appl. Opt.*, 20, 2919-2924, 1981.
- Donelan, M.A., Air-sea interaction, in *Ocean Engineering Science*, edited by B. Le Méhauté and D.M. Hanes, pp. 239-292, John Wiley & Sons, New York, 1990.
- Edlén, B., The dispersion of standard air, *J. Opt. Soc. Amer.*, 43, 339-344, 1953.
- Edlén, B., The refractive index of air, *Meteor.*, 2, 71-80, 1966.
- Edson, J.B., C.W. Fairall, P.G. Mestayer, and S.E. Larsen, A study of the inertial-dissipation method for computing air-sea fluxes, *J. Geophys. Res.*, 96, 10,689-10,711, 1991.

- Fairall, C.W., G.E. Schacher, and K.L. Davidson, Measurements of the humidity structure function parameters C_q^2 and C_{Tq} over the ocean, *Bound-Layer Meteor.*, 19, 81-92, 1980.
- Fairall, C.W., and S.E. Larsen, Inertial dissipation methods and turbulent fluxes at the air ocean interface, *Bound.-Layer Meteor.* 34, 287-301, 1986.
- Fairall, C.W., J.B. Edson, S.E. Larsen, and P.G. Mestayer, Inertial-dissipation air-sea flux measurements: a prototype system using realtime spectral computations, *J. Atmos. Oceanic. Technol.*, 7, 425-453, 1990.
- Fenn, R.W., S.A. Clough, W.O. Gallery, R.E. Good, F.X. Kneizys, J.D. Mill, L.S. Rothman, E.P. Shettle and F.E. Volz, Optical and infrared properties of the atmosphere, in *Handbook of Geophysics and Space Environment*, edited by A.S. Jursa, pp. 18.1-18.80, Air Force Geophysics Laboratory, National Technical Information Service, Springfield USA, 1985.
- Friehe, C.A., J.C. La Rue, F.H. Champagne, C.H. Gibson and G.F. Dreyer, Effects of temperature and humidity fluctuations on the optical refractive index structure in the marine boundary layer, *J. Opt. Soc. Amer.*, 65, 1502-1511, 1975.
- Geernaert, G.L., S.E. Larsen, and F. Hansen, Measurement of the wind stress, heat flux and turbulence intensity during storm conditions over the North Sea, *J. Geophys. Res.*, 92, 13,127-13,139, 1987.
- Geernaert, G.L., Measurements of the angle between the wind vector and wind stress vector in the surface layer over the North Sea, *J. Geophys. Res.*, 93, 8215-8220, 1988.
- Geernaert, G.L., Bulk parameterization for the wind stress and heat fluxes in *Surface waves and fluxes: Current theory*, vol. 1, edited by G.L. Geernaert and W.L. Plant, Kluwer Academic Publishers, Dordrecht 1990.
- Goodman, J.W. *Statistical Optics*, Wiley, New York, 1985.
- Hill, R.J., and G.R. Ochs, Fine calibration of large-aperture optical scintillometers and an optical estimate of inner scale of turbulence, *Appl. Opt.*, 17, 3608-3612, 1978.
- Hill, R.J., Implications of Monin-Obukhov similarity theory for scalar quantities, *J. Atm. Sci.*, 46, 2236-2244, 1989a.
- Hill, R.J., Structure functions and spectra of scalar quantities in the inertial-convective and viscous-convective ranges of turbulence, *J. Atm. Sci.*, 46, 2245-2251, 1989b.

- Hill, R.J., and G.R. Ochs, Inner-scale dependence of scintillation variances measured in weak scintillation, *J. Opt. Soc. Amer. A*, 9, 1406-1411, 1992a.
- Hill, R.J., and G.R. Ochs, Surface-layer similarity of the temperature structure parameter, *J. Atm. Sci.*, 49, 1348-1353, 1992b.
- Hill, R.J., G.R. Ochs, and J.J. Wilson, Measuring surface-layer fluxes of heat and momentum using optical scintillation, *Bound-Layer Meteor.*, 58, 391-408, 1992.
- Hufnagel, R., and N.R. Stanley, Modulation transfer function associated with image transmission through turbulent media, *J. Opt. Soc. Amer.*, 54, 52-61, 1964.
- Hufnagel, R.F., Propagation through Atmospheric Turbulence, in *The Infrared Handbook*, edited by W.L. Wolfe and G.J. Zissis, pp. 6.1-6.56, Office of Naval Research, Dept. of the Navy, Washington, DC, 1978.
- Kohsiek, W., Measuring C_T^2 , C_Q^2 , and C_{TQ} in the unstable surface layer, and relations to the vertical fluxes of heat and moisture, *Bound.-Layer Meteor.*, 24, 89-107, 1982a.
- Kohsiek, W., Optical and in situ measuring of structure parameters relevant to temperature and humidity, and their applications to the measuring of sensible and latent heat flux, *NOAA Technical Memorandum ERL WPL-96*, 64 pp., 1982b.
- Kohsiek, W., and M.H.A.J. Herben, Evaporation derived from optical and radio-wave scintillation, *Appl. Opt.*, 22, 2566-2570, 1983.
- Kunkel, K.E., and D.L. Walters, Modeling the diurnal dependence of the optical refractive index structure parameter, *J. Geophys. Res.*, 88, 10.999-11.004, 1983.
- Kunz, G.J., On lidar signals induced by spatial variability of the atmospheric refractive index, *TNO-Physics and Electronics Laboratory, Report FEL-92-A412*, 1993.
- Large, W.G., and S. Pond, Open ocean momentum flux measurements in moderate to strong winds, *J. Phys. Oceanogr.*, 11, 324-336, 1981.
- Large, W.G., and S. Pond, Sensible and latent heat flux measurements over the ocean, *J. Phys. Oceanogr.*, 12, 464-482, 1982.
- Lawrence R.S., and J.W. Strohbehn, A survey of clear-air propagation effects relevant to optical communications, *Proc. IEEE*, 58, 1523-1545, 1970.
- Lawrence, R.S., G.R. Ochs, and S.F. Clifford, Measurements of atmospheric turbulence relevant to optical propagation, *J. Opt. Soc. Amer.*, 60, 826-830, 1970.
- Makin, V.K., V.N. Kudryavtsev and C. Mastenborek, Drag of the sea surface, *Bound.-Layer Meteor.*, 73, 159-182, 1995.

Ochs, G.R., and T. Wang, Finite aperture scintillometer for profiling wind and C_n^2 , *Appl. Opt.* 17, 3774-3778, 1978.

Owens, J.C., Optical refractive index of air: dependence on pressure, temperature and composition, *Appl. Opt.*, 6, 51-58, 1967.

Panofsky, H.A., and J.A. Dutton, *Atmospheric turbulence: models and methods for engineering applications*, 397 pp., John Wiley & Sons, New York, USA, 1984.

Rojas, C.M., R.E. van Grieken, and R.W. Laane, Comparison of three dry deposition models applied to field measurements in the southern bight of the North Sea, *Atm. Env.*, 27A, 363-370, 1993.

Smith, S.D., Wind stress and heat flux over the ocean in gale force winds, *J. Phys. Oceanogr.*, 10, 709-726, 1980.

Smith, S.D., Factors for adjustment of wind speed over water to a 10-metre height, *Bedford Institute of Oceanography, Report BI-R-81-3*, 1981.

Smith S.D., Coefficients for sea surface wind stress, heat flux, and wind profiles as a function of wind speed and temperature, *J. Geophys. Res.*, 93, 15,467-15,472, 1988.

Smith, S.D., Water vapor flux at the sea surface; Review paper, *Bound.-Layer Meteor.*, 47, 277-293, 1989.

Smith, S.D., R.J. Anderson, E.P. Jones, R.L. Desjardins, R.M. Moore, O. Hertzman, and B.D. Johnson, A new measurement of CO₂ eddy flux in the nearshore atmosphere surface layer, *J. Geophys. Res.*, 96, 8881-8887, 1991.

Smith, S.D., R.J. Anderson, O. Hertzman, and M.-C. Bourque, Eddy correlation measurement of CO₂ flux at the sea surface in ASGASEX, Lisbon Conference 1994.

Smith, S.D., R.J. Anderson, O. Hertzman, W.A. Oost, W. Kohsiek, G de Leeuw, and G.J. Kunz, New measurements of water vapour fluxes at the sea surface, in *Third Symposium on Air-Water Gas Transfer* edited by B. Jähne, Univ. Heidelberg, 1995.

Stull, R.B., *An introduction to boundary layer meteorology*, 666 pp., Kluwer Academic Publishers, Dordrecht, 1988.

Tennekes, H., and J.L. Lumley, *A first course in turbulence*, 300 pp., The MIT Press, Cambridge, Massachusetts, 1972.

Thiermann, V., and A. Kohnle, Modelling of optically and IR effective atmospheric turbulence, in *Atmospheric Propagation in the UV, Visible and IR and mm-wave region and related systems aspects*, pp. 19.1-19.12, Proc. AGARD Symposium No. 44, Copenhagen, Denmark, 1989.

Thomas, M.E.; Duncan, D.D.: Atmospheric transmission. in: *The Infrared & Electro-Optical Systems Handbook, Vol. 2, Atmospheric propagation of radiation*. edited by: Smith, F.G., SPIE, Bellingham, Wa, USA, pp. 1-156, 1993.

Wang, T., G.R. Ochs, and S.F. Clifford, A saturation-resistant optical scintillometer to measure C_n^2 , *J. Opt. Soc. Amer.*, 68, 334-338, 1978.

Wu, J., Wind-stress coefficients over sea surface from breeze to hurricane, *J. Geophys. Res.*, 87, 9704-9706, 1982.

Wyngaard, J.C., Y. Izumi, and S.A. Collins Jr., Behaviour of the refractive-index-structure parameter near the ground, *J. Opt. Soc. Amer.*, 61, 1646-1650, 1971.


Wyngaard, J.C., and M.A. LeMone, Behavior of the refractive index structure parameter in the entraining boundary layer, *J. Atm. Sci.*, 37, 1573-1585, 1980.

Yelland, M.J., P.K. Taylor, I.E., Consterdine, and M.H. Smith, The use of the inertial dissipation technique for shipboard wind stress determination, *J. Atmos. Oceanic. Technol.*, 1093-1108, 1994.

8. Signature

A handwritten signature in black ink, consisting of several fluid, overlapping strokes that form a stylized representation of the name.

C.W. Lamberts
Group leader

A handwritten signature in black ink, featuring a series of connected loops and a long, sweeping tail that ends in a small hook.

G.J. Kunz
Author

Appendix A List of symbols

A	constant; dimensionless;
B	Bowen ratio; dimensionless;
C_D	drag coefficient; dimensionless;
C_{DN}	10 m, neutral drag coefficient; dimensionless;
C_E	exchange coefficient for water vapor; dimensionless;
C_{EN}	10 m, neutral exchange coefficient for water vapor; dimensionless;
C_H	exchange coefficient for heat; dimensionless
C_{HN}	10 m, neutral exchange coefficient for heat; dimensionless;
C_n^2	structure function parameter for refractive index in $m^{-2/3}$;
C_q^2	structure function parameter for specific humidity in $m^{-2/3}$;
C_T^2	structure function parameter for temperature in $K^2 \cdot m^{-2/3}$;
C_{Tq}	covariance structure function in $K \cdot m^{-2/3}$;
$D_{xx}(R)$	structure function of parameter x in square of dimension of x ;
E	Water vapor flux in $kg/(m^2s)$;
F	focal length of the optics in m;
H	sensible heat flux in W/m^2 ;
H_e	Latent heat flux in W/m^2 ;
L	Monin-Obukhov length in m;
L_v	latent heat of vaporization in J/kg ;
τ	momentum flux in N/m^2 ;
N	refractivity; dimensionless;
P_z	pressure in Pa (Pascal) at height z ;
Q_z	specific humidity in kg/kg at height z ;
R_g	universal gas constant in $J/(kmol.K)$;
R	range in m;
T_z	temperature in K at height z ;
U_z	wind speed in m/s at height z ;
a	radius of the optics aperture in m;
b	constant in equation in (3.11b);
c_p	specific heat at constant pressure in $J/(kg.K)$
e	partial water vapor pressure in Pa;
g	acceleration due to gravity in m/s^2 ;
k	von Kármán constant; in this work $k = 0.4$; dimensionless;
m	apparent molecular weight of air in $kmol$;
m_d	molecular weight for dry air in $kmol$;
m_w	molecular weight for wet air in $kmol$;

n	refractive index; dimensionless;
q'	fluctuating part of the specific humidity in kg/kg;
q_*	scaling specific humidity in kg/kg;
r	reference range in m;
t'	fluctuating part of the temperature in K;
t_*	scaling temperature in K;
u'	fluctuating part of the horizontal wind speed in m/s.
u_*	friction velocity in m/s;
w'	fluctuating part of the vertical wind speed in m/s.
z	height above the surface in m;
z_{oq}	roughness length for specific humidity in m;
z_{ot}	roughness length for temperature in m;
z_{ou}	roughness length for wind speed in m;
Θ_v	virtual potential temperature in K;
Θ_z	potential temperature in K at height z ;
λ	optical wavelength in m;
ζ	symbol for z / L , stability; dimensionless;
θ'	fluctuating part of the potential temperature in K;
θ_*	scaling potential temperature in K;
ν	dynamic viscosity; $1.4 \cdot 10^{-6}$ m/s; (thus not symbol ν -second-)
ρ	density of air in kg/m ³ ;
ψ_q	stability correction function for specific humidity; dimensionless;
ψ_t	stability correction function for temperature; dimensionless;
ψ_m	stability correction function for wind speed; dimensionless;

Appendix B Tables with numerical results

The data presented in this appendix are calculated from the model based on a friction velocity controlled roughness length. The format and the sequence of the tables are identical to the tables published by Smith (1988). All the values in the tables differ no more than 1 % from Smith's data except for three indicated values in Table B5-1. Our data is referenced to a 10 m pressure of 1013.25 hPa and a relative humidity of 80 %. The input temperatures have been chosen such that the virtual potential temperature differences, $(T_{vs} - \theta_{vz})$, are within 0.005 °C of Smith (1988). By taking the virtual temperature, the results are independent from relative humidity.

For comparison with the model based on a neutral wind speed controlled neutral drag coefficient, a second set of tables has been added.

Note that the largest difference between the two models, on the order of about 25 %, is found in the momentum flux. For the heat and water vapor fluxes, these differences are only a few percent, except for the values at very low wind speeds.

Table B1-1: 10 m drag coefficients $C_D(10) 10^3$, from wind and temperature measurements at the same height. Model based on z_{0w}

Zou	Drag coefficient $C_D(10) * 1000$					
SATD	WIND SPEED in m/s at 10 m height					
in °C	2	5	10	15	20	25
-20.0	--	--	0.52	1.17	1.58	1.90
-15.0	--	--	0.69	1.27	1.64	1.93
-10.0	--	0.10	0.89	1.36	1.69	1.97
-5.0	--	0.41	1.09	1.46	1.75	2.01
-4.0	--	0.51	1.13	1.48	1.76	2.01
-3.0	--	0.62	1.17	1.50	1.77	2.02
-2.0	0.04	0.75	1.21	1.52	1.78	2.03
-1.0	0.37	0.89	1.26	1.54	1.79	2.04
0.0	1.02	1.04	1.29	1.55	1.80	2.04
1.0	1.20	1.11	1.33	1.57	1.81	2.05
2.0	1.27	1.16	1.35	1.59	1.82	2.05
3.0	1.33	1.19	1.37	1.60	1.83	2.06
4.0	1.37	1.22	1.39	1.61	1.84	2.06
5.0	1.41	1.25	1.41	1.62	1.84	2.07
10.0	1.54	1.34	1.48	1.67	1.88	2.09
15.0	1.62	1.40	1.53	1.71	1.91	2.12
20.0	1.69	1.46	1.57	1.74	1.93	2.14

Table B2-1: 10 m heat exchange coefficients $C_H(10) 10^3$, from wind and temperature measurements at the same height. Model based on z_{0w}

Zou	Heat exchange coef. $C_H(10) * 1E3$					
SATD	WIND SPEED in m/s at 10 m height					
in °C	2	5	10	15	20	25
-20.0	--	--	0.48	0.82	0.92	0.96
-15.0	--	--	0.61	0.87	0.94	0.97
-10.0	--	0.10	0.75	0.92	0.96	0.98
-5.0	--	0.42	0.88	0.96	0.98	0.99
-4.0	--	0.51	0.90	0.97	0.98	0.99
-3.0	--	0.63	0.93	0.98	0.99	0.99
-2.0	0.04	0.75	0.95	0.98	0.99	1.00
-1.0	0.36	0.87	0.98	0.99	1.00	1.00
0.0	1.04	1.01	1.00	1.00	1.00	1.00
1.0	1.31	1.10	1.02	1.01	1.00	1.00
2.0	1.43	1.16	1.04	1.02	1.01	1.00
3.0	1.51	1.20	1.06	1.02	1.01	1.01
4.0	1.58	1.23	1.07	1.03	1.02	1.01
5.0	1.63	1.26	1.09	1.04	1.02	1.01
10.0	1.83	1.36	1.14	1.06	1.03	1.02
15.0	1.96	1.42	1.17	1.08	1.05	1.03
20.0	2.07	1.48	1.20	1.10	1.06	1.03

Table B3-1: 10 m drag coefficients $C_D(10) 10^3$, from wind and temperature measurements at 20 m altitude. Model based on z_{our}

Zou	Drag coefficient $C_D(20) * 1000$					
SATD	WIND SPEED in m/s at 20 m height					
in °C	2	5	10	15	20	25
-20.0	--	--	--	0.53	1.09	1.42
-15.0	--	--	--	0.75	1.20	1.49
-10.0	--	--	0.28	0.95	1.30	1.56
-5.0	--	--	0.72	1.14	1.41	1.62
-4.0	--	--	0.80	1.18	1.43	1.64
-3.0	--	0.13	0.89	1.22	1.45	1.65
-2.0	--	0.36	0.97	1.25	1.47	1.66
-1.0	--	0.64	1.05	1.29	1.49	1.68
0.0	0.94	0.93	1.12	1.32	1.51	1.69
1.0	1.14	1.03	1.17	1.35	1.53	1.70
2.0	1.23	1.08	1.21	1.37	1.54	1.71
3.0	1.28	1.12	1.23	1.39	1.55	1.72
4.0	1.33	1.15	1.26	1.41	1.57	1.73
5.0	1.36	1.18	1.28	1.42	1.58	1.74
10.0	1.49	1.27	1.35	1.48	1.62	1.77
15.0	1.58	1.34	1.41	1.53	1.66	1.80
20.0	1.65	1.39	1.45	1.57	1.70	1.83

Table B4-1: 10 m drag coefficients $C_T(10) 10^3$, from wind and temperature measurements at 20 m altitude. Model based on z_{our}

Zou	Heat exchange coef. $Ch(20) * 1E3$					
SATD	WIND SPEED in m/s at 20 m height					
in °C	2	5	10	15	20	25
-20.0	--	--	--	0.54	0.78	0.85
-15.0	--	--	--	0.67	0.82	0.87
-10.0	--	--	0.36	0.78	0.86	0.89
-5.0	--	--	0.71	0.86	0.90	0.91
-4.0	--	--	0.77	0.88	0.91	0.91
-3.0	--	0.20	0.82	0.89	0.91	0.92
-2.0	--	0.47	0.86	0.91	0.92	0.92
-1.0	--	0.73	0.90	0.92	0.93	0.93
0.0	1.00	0.96	0.94	0.94	0.93	0.93
1.0	1.29	1.07	0.98	0.95	0.94	0.93
2.0	1.41	1.13	1.00	0.96	0.94	0.94
3.0	1.49	1.17	1.02	0.97	0.95	0.94
4.0	1.55	1.20	1.03	0.98	0.95	0.94
5.0	1.61	1.23	1.05	0.99	0.96	0.94
10.0	1.81	1.33	1.10	1.02	0.98	0.96
15.0	1.94	1.40	1.14	1.04	0.99	0.97
20.0	2.05	1.46	1.17	1.06	1.01	0.98

Table B5-1: Ratios of wind speeds at 10 m and 1 m, U_{10}/U_1 , from wind and temperature measurements at 1 m altitude. Model based on z_{out}

Zou	Ratio wind speed $U(10)/U(1)$					
SATD	WIND SPEED in m/s at 1 m height					
in °C	2	4	8	16	24	36
-20.0	7.81	3.00	1.60	1.38	1.42	1.52
-15.0	6.32	2.57	1.52	1.37	1.41	1.52
-10.0	4.76	2.13	1.43	1.36	1.41	1.52
-5.0	3.09	1.68	1.35	1.34	1.40	1.52
-4.0	2.74	1.59	1.33	1.34	1.40	1.52
-3.0	2.38	1.50	1.31	1.34	1.40	1.52
-2.0	2.01	1.41	1.30	1.34	1.40	1.52
-1.0	1.62	1.32	1.28	1.33	1.40	1.52
0.0	--	1.22	1.26	1.33	1.40	1.52
1.0	1.14	1.19	1.25	1.33	1.40	1.52
2.0	1.13	1.17	1.24	1.33	1.40	1.52
3.0	1.12	1.16	1.23	1.32	1.40	1.52
4.0	1.11	1.15	1.23	1.32	1.40	1.52
5.0	1.11	1.15	1.22	1.32	1.40	1.52
10.0	1.09	1.13	1.21	1.31	1.39	1.52
15.0	1.09	1.12	1.19	1.31	1.39	1.52
20.0	1.08	1.12	1.19	1.30	1.39	1.52

Table B6-1: Ratios of wind speeds at 10 m and 2 m, U_{10}/U_2 , from wind and temperature measurements at 2 m altitude. Model based on z_{out}

Zou	Ratio wind speed $U(10)/U(2)$					
SATD	WIND SPEED in m/s at 2 m height					
in °C	2	4	8	16	24	36
-20.0	--	2.73	1.49	1.26	1.25	1.29
-15.0	--	2.35	1.41	1.24	1.25	1.29
-10.0	4.17	1.96	1.33	1.23	1.25	1.29
-5.0	2.74	1.56	1.25	1.22	1.24	1.29
-4.0	2.45	1.48	1.23	1.21	1.24	1.29
-3.0	2.14	1.40	1.21	1.21	1.24	1.29
-2.0	1.82	1.31	1.20	1.21	1.24	1.29
-1.0	1.49	1.23	1.18	1.21	1.24	1.29
0.0	1.14	1.14	1.17	1.20	1.24	1.29
1.0	1.09	1.12	1.16	1.20	1.24	1.29
2.0	1.08	1.10	1.15	1.20	1.24	1.29
3.0	1.07	1.10	1.14	1.20	1.23	1.29
4.0	1.07	1.09	1.14	1.20	1.23	1.29
5.0	1.07	1.09	1.14	1.19	1.23	1.29
10.0	1.06	1.08	1.12	1.19	1.23	1.29
15.0	1.05	1.07	1.12	1.18	1.23	1.28
20.0	1.05	1.07	1.11	1.18	1.23	1.28

Table B7-1: Ratios of wind speeds at 10 m and 5 m, U_{10}/U_5 , from wind and temperature measurements at 5 m altitude. Model based on z_{ow} .

Zou	Ratio wind speed $U(10)/U(5)$					
SATD	WIND SPEED in m/s at 5 m height					
in °C	2	4	8	16	24	36
-20.0	--	--	1.29	1.11	1.10	1.10
-15.0	--	1.78	1.23	1.10	1.10	1.10
-10.0	--	1.56	1.17	1.09	1.09	1.10
-5.0	--	1.32	1.12	1.09	1.09	1.10
-4.0	1.83	1.26	1.11	1.08	1.09	1.10
-3.0	1.64	1.21	1.10	1.08	1.09	1.10
-2.0	1.46	1.16	1.08	1.08	1.09	1.10
-1.0	1.26	1.11	1.07	1.08	1.09	1.10
0.0	1.05	1.06	1.06	1.08	1.09	1.10
1.0	1.03	1.04	1.06	1.07	1.09	1.10
2.0	1.03	1.04	1.05	1.07	1.09	1.10
3.0	1.03	1.04	1.05	1.07	1.08	1.10
4.0	1.02	1.03	1.05	1.07	1.08	1.10
5.0	1.02	1.03	1.05	1.07	1.08	1.10
10.0	1.02	1.03	1.04	1.07	1.08	1.10
15.0	1.02	1.03	1.04	1.06	1.08	1.10
20.0	1.02	1.03	1.04	1.06	1.08	1.10

Table B8-1: Ratios of wind speeds at 20 m and 10 m, U_{20}/U_{10} , from wind and temperature measurements at 20 m altitude. Model based on z_{ow} .

Zou	Ratio wind speed $U(20)/U(10)$					
SATD	WIND SPEED in m/s at 20 m height					
in °C	2	4	8	16	24	36
-20.0	--	--	--	0.85	0.90	0.91
-15.0	--	--	0.57	0.87	0.91	0.91
-10.0	--	--	0.70	0.89	0.92	0.92
-5.0	--	--	0.83	0.92	0.92	0.92
-4.0	--	0.57	0.85	0.92	0.92	0.92
-3.0	--	0.66	0.88	0.92	0.93	0.92
-2.0	--	0.76	0.90	0.93	0.93	0.92
-1.0	0.62	0.86	0.92	0.93	0.93	0.92
0.0	0.96	0.95	0.95	0.94	0.93	0.92
1.0	0.97	0.97	0.95	0.94	0.93	0.92
2.0	0.98	0.97	0.96	0.94	0.93	0.92
3.0	0.98	0.97	0.96	0.94	0.93	0.92
4.0	0.98	0.97	0.96	0.94	0.93	0.92
5.0	0.98	0.98	0.96	0.95	0.93	0.92
10.0	0.98	0.98	0.97	0.95	0.94	0.92
15.0	0.98	0.98	0.97	0.95	0.94	0.93
20.0	0.98	0.98	0.97	0.95	0.94	0.93

Table B1-2: 10 m drag coefficients $C_D(10)10^3$, from wind and temperature measurements at the same height. Model based on C_{DN} .

Cdn	Drag coefficient $C_D(10)*1000$					
SATD	WIND SPEED in m/s at 10 m height					
in °C	2	5	10	15	20	25
-20.0	--	--	0.55	1.43	2.04	2.55
-15.0	--	--	0.76	1.54	2.10	2.59
-10.0	--	0.04	0.98	1.64	2.16	2.63
-5.0	--	0.32	1.20	1.75	2.22	2.67
-4.0	--	0.43	1.25	1.77	2.23	2.67
-3.0	--	0.55	1.30	1.79	2.24	2.68
-2.0	0.01	0.69	1.34	1.81	2.26	2.69
-1.0	0.16	0.85	1.39	1.84	2.27	2.70
0.0	0.78	1.01	1.43	1.86	2.28	2.71
1.0	0.95	1.09	1.46	1.87	2.29	2.71
2.0	1.02	1.14	1.49	1.89	2.30	2.72
3.0	1.07	1.18	1.51	1.90	2.31	2.72
4.0	1.11	1.21	1.54	1.91	2.32	2.73
5.0	1.14	1.24	1.55	1.93	2.33	2.74
10.0	1.25	1.34	1.63	1.98	2.36	2.76
15.0	1.34	1.41	1.69	2.03	2.40	2.79
20.0	1.40	1.46	1.74	2.07	2.43	2.81

Table B2-2: 10 m heat exchange coefficients $C_H(10)10^3$, from wind and temperature measurements at the same height. Model based on C_{DN} .

Cdn	Heatexchange coef. $C_H(10)*1E3$					
SATD	WIND SPEED in m/s at 10 m height					
in °C	2	5	10	15	20	25
-20.0	--	--	0.50	0.86	0.94	0.97
-15.0	--	--	0.64	0.90	0.96	0.98
-10.0	--	0.05	0.77	0.93	0.97	0.99
-5.0	--	0.35	0.89	0.97	0.99	0.99
-4.0	--	0.47	0.91	0.97	0.99	0.99
-3.0	--	0.59	0.94	0.98	0.99	1.00
-2.0	0.01	0.73	0.96	0.99	0.99	1.00
-1.0	0.19	0.87	0.98	0.99	1.00	1.00
0.0	1.06	1.01	1.00	1.00	1.00	1.00
1.0	1.41	1.10	1.02	1.01	1.00	1.00
2.0	1.55	1.16	1.04	1.01	1.01	1.00
3.0	1.65	1.20	1.05	1.02	1.01	1.00
4.0	1.73	1.23	1.07	1.02	1.01	1.01
5.0	1.79	1.26	1.08	1.03	1.01	1.01
10.0	2.03	1.36	1.12	1.05	1.02	1.01
15.0	2.20	1.42	1.15	1.07	1.03	1.02
20.0	2.33	1.48	1.18	1.08	1.04	1.02

Table B3-2: 10 m drag coefficients $C_D(10)10^3$, from wind and temperature measurements at 20 m altitude. Model based on C_{DN} .

Cdn	Drag coefficient $C_D(20)*1000$					
SATD	WIND SPEED in m/s at 20 m height					
in °C	2	5	10	15	20	25
-20.0	--	--	--	0.67	1.39	1.86
-15.0	--	--	--	0.92	1.51	1.93
-10.0	--	--	0.26	1.14	1.62	2.00
-5.0	--	--	0.78	1.34	1.74	2.07
-4.0	--	--	0.87	1.38	1.76	2.09
-3.0	--	0.03	0.96	1.42	1.78	2.10
-2.0	--	0.25	1.05	1.46	1.80	2.12
-1.0	--	0.58	1.14	1.50	1.82	2.13
0.0	0.72	0.90	1.22	1.54	1.85	2.14
1.0	0.91	1.01	1.27	1.57	1.86	2.16
2.0	0.98	1.06	1.31	1.59	1.88	2.17
3.0	1.03	1.10	1.34	1.61	1.89	2.18
4.0	1.07	1.14	1.37	1.63	1.91	2.19
5.0	1.10	1.16	1.39	1.65	1.92	2.19
10.0	1.22	1.26	1.48	1.72	1.97	2.24
15.0	1.30	1.34	1.54	1.78	2.02	2.28
20.0	1.37	1.39	1.59	1.82	2.06	2.31

Table B4-2: 10 m drag coefficients $C_T(10)10^3$, from wind and temperature measurements at 20 m altitude. Model based on C_{DN} .

Cdn	Heat exchange coef. $Ch(20)*1E3$					
SATD	WIND SPEED in m/s at 20 m height					
in °C	2	5	10	15	20	25
-20.0	--	--	--	0.59	0.81	0.86
-15.0	--	--	--	0.71	0.84	0.88
-10.0	--	--	0.35	0.80	0.87	0.89
-5.0	--	--	0.73	0.87	0.90	0.91
-4.0	--	--	0.78	0.88	0.91	0.91
-3.0	--	0.06	0.82	0.90	0.91	0.91
-2.0	--	0.38	0.87	0.91	0.92	0.91
-1.0	--	0.71	0.91	0.92	0.92	0.92
0.0	1.03	0.96	0.94	0.93	0.93	0.92
1.0	1.39	1.07	0.97	0.94	0.93	0.92
2.0	1.53	1.13	0.99	0.95	0.93	0.92
3.0	1.63	1.17	1.01	0.96	0.94	0.93
4.0	1.71	1.21	1.02	0.97	0.94	0.93
5.0	1.78	1.23	1.04	0.97	0.95	0.93
10.0	2.02	1.33	1.08	1.00	0.96	0.94
15.0	2.19	1.40	1.12	1.02	0.97	0.95
20.0	2.32	1.46	1.15	1.04	0.99	0.96

Table B5-2: Ratios of wind speeds at 10 m and 1 m, U_{10}/U_1 , from wind and temperature measurements at 1 m altitude. Model based on C_{DN} .

Cdn	Ratio wind speed $U(10)/U(1)$					
SATD	WIND SPEED in m/s at 1 m height					
in °C	2	4	8	16	24	36
-20.0	8.61	3.15	1.58	1.44	1.55	1.83
-15.0	7.25	2.67	1.51	1.43	1.55	1.83
-10.0	5.60	2.18	1.43	1.42	1.55	1.83
-5.0	3.61	1.70	1.36	1.41	1.54	1.82
-4.0	3.17	1.61	1.34	1.41	1.54	1.82
-3.0	2.71	1.51	1.33	1.41	1.54	1.82
-2.0	2.23	1.41	1.31	1.41	1.54	1.82
-1.0	1.73	1.32	1.30	1.40	1.54	1.82
0.0	1.20	1.22	1.28	1.40	1.54	1.82
1.0	1.12	1.18	1.27	1.40	1.54	1.82
2.0	1.10	1.17	1.26	1.40	1.54	1.82
3.0	1.10	1.16	1.26	1.40	1.54	1.82
4.0	1.09	1.15	1.25	1.40	1.54	1.82
5.0	1.09	1.14	1.25	1.40	1.54	1.82
10.0	1.08	1.13	1.23	1.39	1.54	1.82
15.0	1.07	1.12	1.22	1.38	1.54	1.82
20.0	1.07	1.11	1.21	1.38	1.53	1.82

Table B6-2: Ratios of wind speeds at 10 m and 2 m, U_{10}/U_2 , from wind and temperature measurements at 2 m altitude. Model based on C_{DN} .

Cdn	Ratio wind speed $U(10)/U(2)$					
SATD	WIND SPEED in m/s at 2 m height					
in °C	2	4	8	16	24	36
-20.0	--	2.91	1.47	1.28	1.31	1.39
-15.0	--	2.48	1.40	1.27	1.30	1.39
-10.0	4.49	2.04	1.32	1.26	1.30	1.39
-5.0	3.11	1.59	1.25	1.25	1.30	1.39
-4.0	2.77	1.50	1.23	1.24	1.30	1.39
-3.0	2.41	1.41	1.22	1.24	1.30	1.39
-2.0	2.01	1.32	1.20	1.24	1.30	1.39
-1.0	1.59	1.23	1.19	1.24	1.30	1.39
0.0	1.12	1.14	1.18	1.24	1.30	1.39
1.0	1.07	1.11	1.17	1.24	1.30	1.39
2.0	1.06	1.10	1.16	1.23	1.30	1.39
3.0	1.06	1.09	1.15	1.23	1.29	1.39
4.0	1.06	1.09	1.15	1.23	1.29	1.39
5.0	1.05	1.09	1.15	1.23	1.29	1.39
10.0	1.05	1.08	1.13	1.22	1.29	1.39
15.0	1.04	1.07	1.13	1.22	1.29	1.39
20.0	1.04	1.07	1.12	1.22	1.29	1.39

Table B7-2: Ratios of wind speeds at 10 m and 5 m, U_{10}/U_5 , from wind and temperature measurements at 5 m altitude. Model based on C_{DN} .

Cdn	Ratio wind speed $U(10)/U(5)$					
SATD	WIND SPEED in m/s at 5 m height					
in °C	2	4	8	16	24	36
-20.0	--	--	1.29	1.11	1.11	1.13
-15.0	--	1.84	1.23	1.11	1.11	1.13
-10.0	--	1.61	1.17	1.10	1.11	1.12
-5.0	--	1.34	1.12	1.09	1.10	1.12
-4.0	1.90	1.28	1.11	1.09	1.10	1.12
-3.0	1.74	1.23	1.10	1.09	1.10	1.12
-2.0	1.55	1.17	1.09	1.09	1.10	1.12
-1.0	1.32	1.11	1.08	1.09	1.10	1.12
0.0	1.04	1.05	1.07	1.09	1.10	1.12
1.0	1.03	1.04	1.06	1.08	1.10	1.12
2.0	1.02	1.04	1.06	1.08	1.10	1.12
3.0	1.02	1.03	1.05	1.08	1.10	1.12
4.0	1.02	1.03	1.05	1.08	1.10	1.12
5.0	1.02	1.03	1.05	1.08	1.10	1.12
10.0	1.02	1.03	1.05	1.08	1.10	1.12
15.0	1.02	1.03	1.04	1.07	1.10	1.12
20.0	1.02	1.02	1.04	1.07	1.10	1.12

Table B8-2: Ratios of wind speeds at 20 m and 10 m, U_{20}/U_{10} , from wind and temperature measurements at 20 m altitude. Model based on C_{DN} .

Cdn	Ratio wind speed $U(20)/U(10)$					
SATD	WIND SPEED in m/s at 20 m height					
in °C	2	4	8	16	24	36
-20.0	--	--	--	0.85	0.90	0.90
-15.0	--	--	0.55	0.88	0.90	0.90
-10.0	--	--	0.68	0.90	0.91	0.91
-5.0	--	--	0.83	0.91	0.92	0.91
-4.0	--	0.54	0.86	0.92	0.92	0.91
-3.0	--	0.63	0.88	0.92	0.92	0.91
-2.0	--	0.74	0.90	0.92	0.92	0.91
-1.0	0.59	0.85	0.92	0.93	0.92	0.91
0.0	0.97	0.95	0.94	0.93	0.92	0.91
1.0	0.98	0.97	0.95	0.93	0.92	0.91
2.0	0.98	0.97	0.96	0.93	0.92	0.91
3.0	0.98	0.97	0.96	0.94	0.92	0.91
4.0	0.98	0.98	0.96	0.94	0.92	0.91
5.0	0.98	0.98	0.96	0.94	0.92	0.91
10.0	0.99	0.98	0.97	0.94	0.93	0.91
15.0	0.99	0.98	0.97	0.95	0.93	0.91
20.0	0.99	0.98	0.97	0.95	0.93	0.91

Appendix C Short sensitivity analysis

C.1 Introduction

Two models were developed to estimate micrometeorological parameters such as fluxes, exchange coefficients and roughness lengths from standard meteorological observations. The models are used to estimate and predict optical and infrared turbulence over the sea. The first model is based on a generally assumed linear relation between the 10 m neutral drag coefficient and the wind speed (Geernaert, 1990) that depends on water depth whereas the other model is based on the relation between the friction velocity and the combined Charnock-Businger roughness length for momentum (Smith 1988). Comparison of the results provided by the two models showed large differences in the roughness lengths and the drag coefficients which resulted in a smaller variation in the friction velocity, an essential normalization parameter. A brief analysis was carried out to study this reduction in sensitivity.

C.2 Sensitivity Analysis

C.2.1 Sensitivity of the roughness length on the drag coefficient

Start with the equation for the vertical wind profile:

$$U = \frac{u_*}{k} \left[\ln\left(\frac{z}{z_{ou}}\right) - \psi_m\left(\frac{z}{L}\right) \right] \quad (C.1)$$

and the definition of the drag coefficient:

$$C_D = \frac{u_*^2}{U^2} \quad (C.2)$$

The dependence of the drag coefficient on the roughness length is expressed in the first derivative of C_D with respect to z_{ou} . This is realized by eliminating U from the equations (C.1) and (C.2) and differentiating to z_{ou} while assuming that the correction term 'psi' is independent on C_D . This results in:

$$\frac{d\sqrt{C_D}}{dz_{ou}} = \frac{C_D}{k z_{ou}} \quad (C.3)$$

This equation can be written as:

$$\frac{d C_D}{C_D} = \frac{2\sqrt{C_D}}{k} \frac{dz_{ou}}{z_{ou}} \quad (C.4)$$

Because C_D varies from about $1.0 \cdot 10^{-3}$ to $2.5 \cdot 10^{-3}$ and $k \approx 0.4$, the numerical value of the first term on the right hand side of (C.4) is about 0.19 (0.12 ... 0.25) for $C_D = 1.5 \cdot 10^{-3}$. This means that, considering this simple analysis without taking into account the variations of the stability, the relative variations in C_D due to small variations in z_{ou} are reduced by a about a factor 5.

In a similar approach, the dependence of the heat and water vapor exchange coefficients on their respective roughness lengths, z_{ot} and z_{oq} , can be estimated.

C.2.2 Sensitivity of the roughness length on the friction velocity

The sensitivity of the friction velocity, u_* , for variations of z_{ou} is found by explicitly writing u_* from equation (C.1) and differentiating to z_{ou} . It is not difficult to see that:

$$\frac{du_*}{dz_{ou}} = \frac{-k U}{\left[\ln\left(\frac{z}{z_{ou}}\right) - \psi_m \right]^2} \cdot \frac{z_{ou}}{z} \cdot \frac{-z}{z_{ou}^2} \quad (C.5)$$

which can be simplified to:

$$\frac{du_*}{dz_{ou}} = \frac{u_*}{k U} \frac{1}{z_{ou}} \quad (C.6)$$

Using (C.2), equation (C.6) can be rewritten as:

$$\frac{du_*}{u_*} = \frac{\sqrt{C_D}}{k} \frac{dz_{ou}}{z_{ou}} \quad (C.7)$$

Note that the first term on the right hand side of this equation differs only a factor of 2 from the first term on the right hand side of equation (C.4). Therefore, its numerical value is about 0.1. This means that the variations in the friction velocity due to variations in the roughness length are reduced by about one order of magnitude.

In a similar approach, the sensitivity of T_* and q_* on respectively z_{ot} and z_{oq} can be estimated. Because C_H and C_q have about the same numerical value as C_D the results will be comparable.

C.2.3 Sensitivity of the neutral drag coefficient on variations of the roughness length

For comparison of data from different heights and recorded under different conditions, results are converted to the standard 10 m altitude under neutral conditions. This can be done by using equation (C.1) given the measured wind speed, U , the friction velocity, u_* , and the correction function for stability, ϕ , which vanishes under neutral conditions (the stability is derived in combination with data from thermometers and hygrometers). As a result, an equation is left that

relates the roughness length with the neutral drag coefficient, $C_{DN}(10)$, generally written as C_{DN} . Thus starting with equation (C.1), the 10 m wind speed becomes:

$$U(10) = \frac{u_*}{k} \left[\ln\left(\frac{10}{z_{ou}}\right) - \psi_m\left(\frac{10}{L}\right) \right] \quad (C.8)$$

Before deriving the neutral drag coefficient it is noticed that converting equation (C.8) to its neutral counter part, changes either $U(10)$ to $U_N(10)$ as given by Anderson (1993) or it changes u_* to u_{*N} as used by Geernaert (1990) (or both, not found in literature). Thus one can write:

$$\sqrt{C_{DN}} = \frac{u_{*N}}{U(10)} = \frac{u_*}{U_N(10)} = \frac{k}{\left(\ln\left(\frac{10}{z_{ou}}\right) - \psi_m\left(\frac{10}{L}\right) \right)} \quad (C.9)$$

Expressing the ratio of the wind speed and the friction velocity in (C.9) in a similar way as in equation (C.2), the neutral drag coefficient C_{DN} becomes:

$$C_{DN} = \frac{k^2}{\left(\ln\left(\frac{10}{z_{ou}}\right) \right)^2} \quad (C.10)$$

C_{DN} depends on the wind speed and is used in many micrometeorological bulk models. It is clear that equation (C.10) can be used as an alternative to express the roughness length.

Also the roughness length is sometimes used as the controlling parameter for bulk models (Smith, 1988). The roughness length is defined as:

$$z_{ou} = \frac{0.011 u_*^2}{g} + \frac{0.11 \nu}{u_*} \quad (C.11)$$

and thus is C_{DN} the dependent parameter. The variation of the neutral drag coefficient with variations of the roughness length can easily be calculated by taking the first derivative of equation (C.10). Applying the chain rule, gives:

$$\frac{dC_{DN}}{dz_{ou}} = 2 \cdot \frac{k}{\ln\left(\frac{10}{z_{ou}}\right)} \cdot \frac{-k}{\left(\ln\left(\frac{10}{z_{ou}}\right) \right)^2} \cdot \frac{z_{ou}}{10} \cdot \frac{-10}{z_{ou}^2} \quad (C.12)$$

Re-ordering and rewriting the equation in terms of relative variations gives:

$$\frac{dC_{DN}}{C_{DN}} = \frac{1}{2} \cdot \frac{1}{\ln\left(\frac{10}{z_{ou}}\right)} \cdot \frac{dz_{ou}}{z_{ou}} \quad (C.13)$$

Because z_{ou} varies from 10^{-6} to 10^{-4} this results in a relative variation of the neutral drag coefficient of about:

$$\frac{dC_{DN}}{C_{DN}} \approx 0.03 \cdot \frac{dz_{ou}}{z_{ou}} \quad (C.14)$$

Thus the relative variations in C_{DN} due to relative variations in z_{ou} are reduced by about a factor 30.

C.2.4 Sensitivity of the friction velocity on the neutral drag coefficient

Before deriving the sensitivity of u_* on variations of C_{DN} , an expression is derived that relates C_D to C_{DN} . Starting with equation (C.1), one can write:

$$\frac{U(10)}{u_*} = \frac{\ln(\frac{10}{z_{ou}})}{k} - \frac{\psi_m(\frac{10}{L})}{k} \quad (C.15)$$

Substitution of (C.2) and (C.10) gives an equation that is often found in literature but written differently here:

$$\frac{1}{\sqrt{C_D}} = \frac{1}{\sqrt{C_{DN}}} - \frac{\psi_m(\frac{10}{L})}{k} \quad (C.16)$$

The sensitivity analysis starts with the equation for the wind profile (C.1) while substituting equation (C.10) for the 'roughness length'. After re-ordering of the parameters, this results in:

$$u_* = \frac{U}{\frac{1}{\sqrt{C_{DN}}} - \frac{\psi_m(\frac{z}{L})}{k}} \quad (C.17)$$

Differentiation of this equation to C_{DN} provides:

$$\frac{du_*}{dC_{DN}} = \frac{U^2}{\left[\frac{1}{\sqrt{C_{DN}}} - \frac{\psi_m(\frac{z}{L})}{k} \right]^2} \cdot \frac{1}{U} \cdot \frac{-1}{2 C_{DN} \sqrt{C_{DN}}} \quad (C.18)$$

Re-ordering of this equation leads to:

$$\frac{du_*}{u_*} = -\frac{1}{2} \cdot \sqrt{\frac{C_D}{C_{DN}}} \cdot \frac{dC_{DN}}{C_{DN}} \quad (C.19)$$

Assuming that, to a first approximation, the middle term is about 1 it can be stated that the relative variations of the drag coefficients are reduced by about a factor 2.

C.3 Conclusion

A brief sensitivity analysis has shown that:

- relative variations in the drag coefficient due to relative variations of the roughness length are reduced by about a factor of 5
- relative variations in the friction velocity due to relative variation of the roughness length are reduced by about one order of magnitude;
- relative variations in the neutral drag coefficient due to relative variations in the roughness length are reduced by about a factor of 30
- relative variations in the neutral drag coefficients due to relative variations of the friction velocity are reduction by about a factor of 2
- the drag coefficient is more sensitive to the roughness length than the neutral drag coefficient

Appendix D Fluxes of momentum, heat and water vapor as a function of wind speed and air-sea temperature difference

In this appendix, figures are presented of the fluxes of momentum, heat and water vapor as a function of wind speed and air-sea temperature difference. The relative humidity is 80 % and the sea surface temperature is 10 °C. The relative humidity directly above the sea surface is 98 %. The following exchange coefficients were selected: neutral drag coefficient of $C_{DN} = (0.58 + 0.085 U_{10N}) 10^{-3}$ (North Sea tower values), Stanton number $C_{HN} = 1.0 \cdot 10^{-3}$ and Dalton number $C_{EN} = 1.2 \cdot 10^{-3}$.

Note that the largest difference between the two models is about 25 % for the momentum flux. For heat and water vapor flux, these differences are of the order of a few percent only, except for the very low wind speed, when the differences between the exchange coefficients become more pronounced.

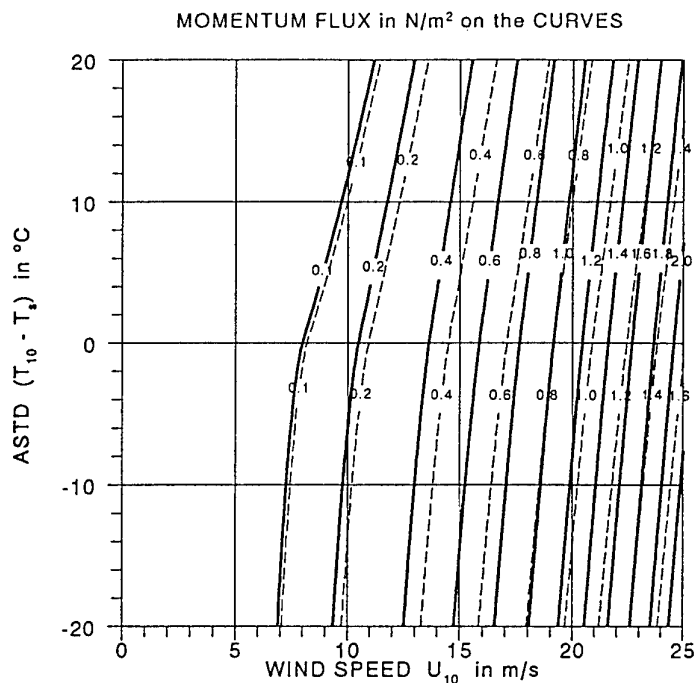


Fig. D1: Momentum flux as a function of wind speed and air-sea temperature-difference both at the standard height of 10 m. The solid curves are from the model based on C_{DN} and the dashed curves are from the model based on z_{0H} .

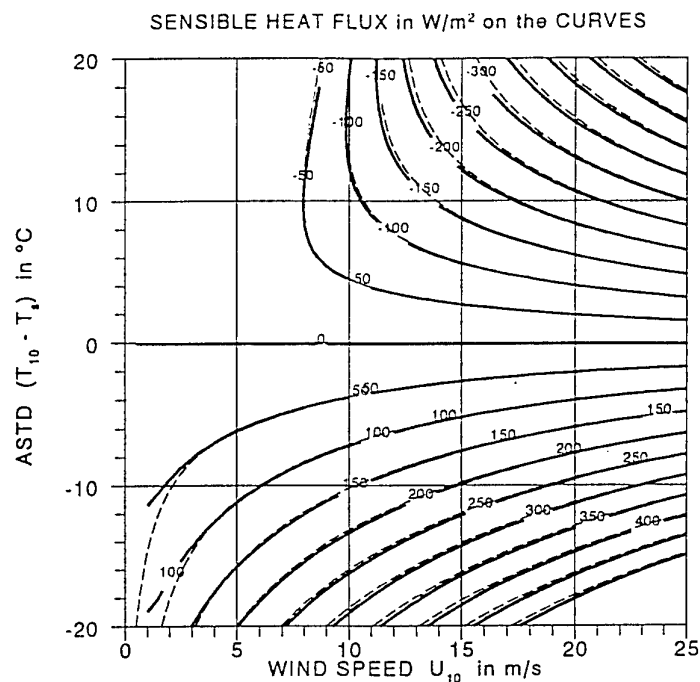


Fig. D2: Sensible heat flux as a function of wind speed and air-sea temperature-difference both at the standard height of 10 m. The solid curves are from the model based on C_{DN} and the dashed curves are from the model based on z_{0ur} .

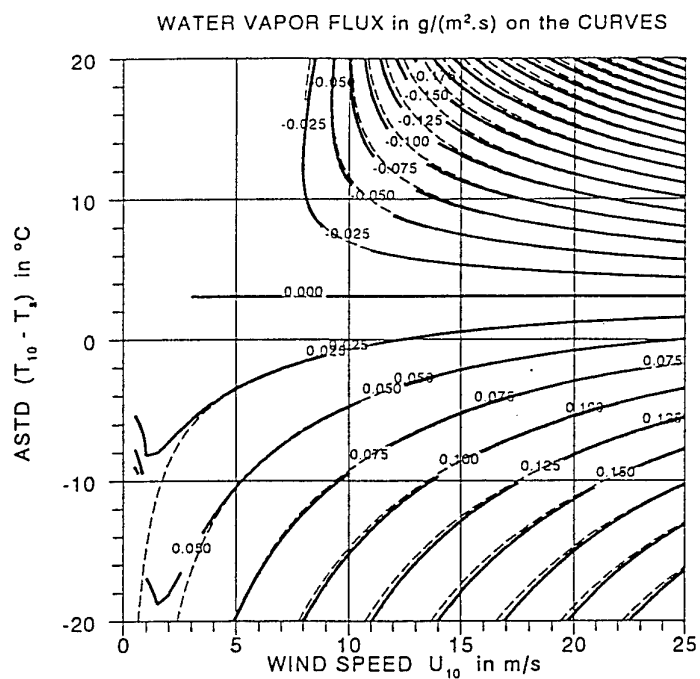


Fig. D3: Water vapor flux as a function of wind speed and air-sea temperature-difference both at the standard height of 10 m. The solid curves are from the model based on C_{DN} and the dashed curves are from the model based on z_{0ur} .

Appendix E Specific humidity versus relative humidity and air temperature

Internally, the micrometeorological model presented in this report, uses the specific humidity whereas the relative humidity is used as input parameter. The figure in this appendix can be helpful to convert or to estimate the actual air temperature and relative humidity to specific humidity. (The specific humidity is the ratio of the mass of water in a volume air and the total mass - dry plus wet- of that volume.)

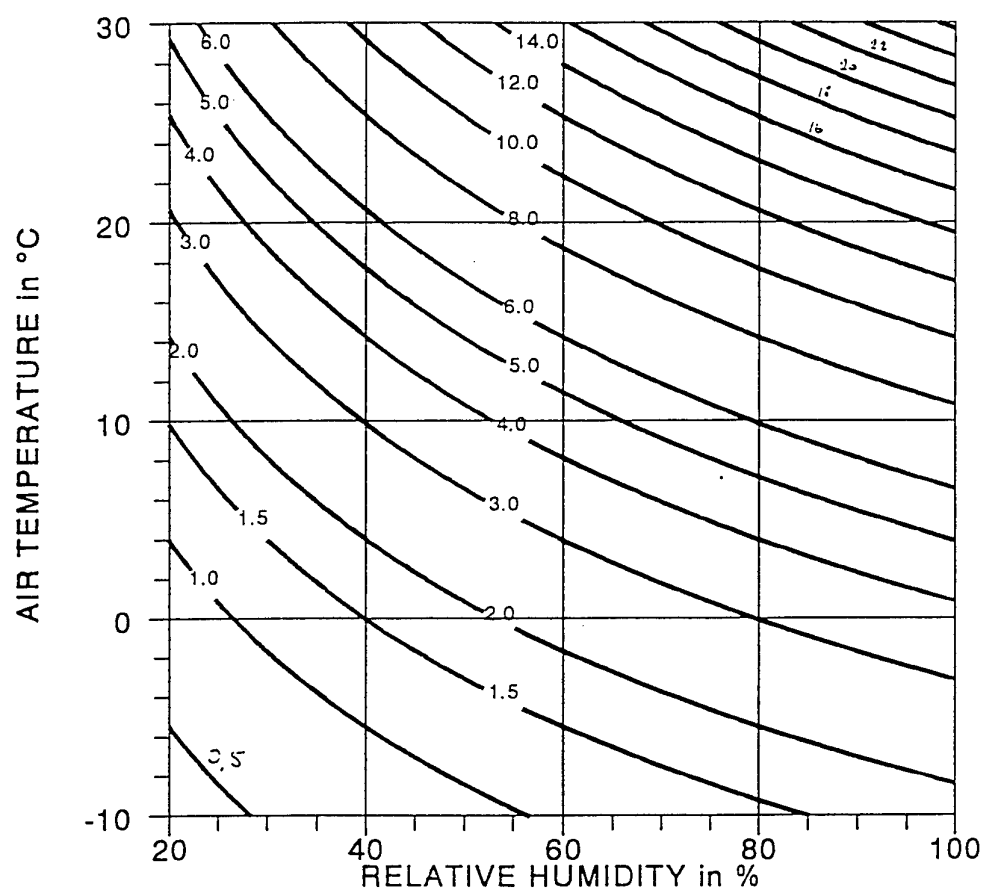


Fig. E1: Specific humidity in g/kg, as a function of air temperature and relative humidity both at the standard height of 10 m. The solid curves are from the model based on C_{DN} and the dashed curves are from the model based on z_{0w} .

ONGERUBRICEERD
REPORT DOCUMENTATION PAGE
(MOD-NL)

1. DEFENCE REPORT NO (MOD-NL) TD96-0381	2. RECIPIENT'S ACCESSION NO	3. PERFORMING ORGANIZATION REPORT NO FEL-96-A053		
4. PROJECT/TASK/WORK UNIT NO 24581	5. CONTRACT NO A94KM786	6. REPORT DATE April 1996		
7. NUMBER OF PAGES 73 (incl 5 appendices, excl RDP & distribution list)	8. NUMBER OF REFERENCES 60	9. TYPE OF REPORT AND DATES COVERED		
10. TITLE AND SUBTITLE A bulk model to predict optical turbulence in the marine surface layer				
11. AUTHOR(S) G.J. Kunz				
12. PERFORMING ORGANIZATION NAME(S) AND ADDRESS(ES) TNO Physics and Electronics Laboratory, PO Box 96864, 2509 JG The Hague, The Netherlands Oude Waalsdorperweg 63, The Hague, The Netherlands				
13. SPONSORING AGENCY NAME(S) AND ADDRESS(ES) Royal Netherlands Navy DMKM/WCS/COSPON, Van der Burchlaan 31, 2597 PC The Hague, The Netherlands				
14. SUPPLEMENTARY NOTES The classification designation Ongerubriceerd is equivalent to Unclassified, Stg. Confidentieel is equivalent to Confidential and Stg. Geheim is equivalent to Secret.				
15. ABSTRACT (MAXIMUM 200 WORDS (1044 BYTE)) A model for turbulence in the marine atmospheric surface layer has been developed and evaluated. The model uses only standard meteorological parameters and is suited to become part of a technical decision aid to predict optical turbulence and refractivity effects. In addition, the model provides all the basic tools to calculate the vertical profiles of wind speed, air temperature and air humidity, the micrometeorological parameters such as stability, roughness lengths, exchange coefficients and the fluxes of momentum, heat, water vapor. These results are used to estimate the structure function parameters for the refractive index, C_n^2 , which is the controlling parameter for the prediction of scintillation, blurring and beam wander.				
<table style="width: 100%; border: none;"><tr><td style="width: 40%; vertical-align: top;">16. DESCRIPTORS Maritime environments Turbulent boundary layer Micrometeorology Clear models air turbulence</td><td style="width: 60%; vertical-align: top;">IDENTIFIERS</td></tr></table>			16. DESCRIPTORS Maritime environments Turbulent boundary layer Micrometeorology Clear models air turbulence	IDENTIFIERS
16. DESCRIPTORS Maritime environments Turbulent boundary layer Micrometeorology Clear models air turbulence	IDENTIFIERS			
17a. SECURITY CLASSIFICATION (OF REPORT) Ongerubriceerd	17b. SECURITY CLASSIFICATION (OF PAGE) Ongerubriceerd	17c. SECURITY CLASSIFICATION (OF ABSTRACT) Ongerubriceerd		
18. DISTRIBUTION AVAILABILITY STATEMENT Unlimited distribution		17d. SECURITY CLASSIFICATION (OF TITLES) Ongerubriceerd		

ONGERUBRICEERD

Distributielijst

1. Bureau TNO Defensieonderzoek
2. Directeur Wetenschappelijk Onderzoek en Ontwikkeling *)
3. HWO-KL *)
4. HWO-KLu *)
5. HWO-KM
6. HWO-CO *)
- 7 t/m 9. KMA, Bibliotheek
10. DMKM/WCS, t.a.v. Ltz M.A. Simmeren
11. DMKM/WCS/EMDC/NAVG, t.a.v. Ing. H. Quik
12. DMKM/WCS/COSPON, t.a.v. Drs. W. Pelt
13. DMKL/AB, t.a.v. Dr. T. van Ittersum
14. DMKL/AT&WO, t.a.v. Ir. N. Pos
15. MARSTAF/OBS/SEWACO
16. KMA, t.a.v. Ir. J. Rogge
17. KIM, t.a.v. Kltz Rademakers
18. Hydrografie/METOC
19. Environment, Canada, t.a.v. Dr. M. Donelan
20. Dr. D. Dion, Dr. L. Forand en Dr. D.L. Hutt, DREV, Canada (1 ex.)
21. BIO, Canada, t.a.v. Dr. S.D. Smith
22. NERI, Denmark, t.a.v. Dr. G.L. Geernaert
23. RISO, Denmark, t.a.v. Dr. F.Aa. Hansen en Dr. S.E. Larsen
24. ECN, France, t.a.v. Prof. Dr. P. Mestayer
25. FfO, Germany, t.a.v. Dr. A. Kohnle
26. Scintec, Germany, t.a.v. Dr. V. Thierman
27. School of the Environment, UK, t.a.v. Dr. M.H. Smith
28. NPS, USA, t.a.v. Prof.dr. K.L. Davidson
29. NCCOSC, USA, t.a.v. Dr. S.G. Gathman en Dr. D.R. Jensen (via De Leeuw)
30. John Hopkins University, MD, USA, t.a.v. Dr. J.P. Reilly (via Schwering)
31. Signaal, t.a.v. Ir. L.H.P. Janssen en Drs. A.C.M. Wagenaar
32. KNMI, t.a.v. Dr. W. Oost
33. VU, Amsterdam, t.a.v. Ir. N.J. Bink
34. VU, Amsterdam, t.a.v. Prof.dr.ir. H. Tennekes
35. Directie TNO-FEL, t.a.v. Dr. J.W. Maas
36. Directie TNO-FEL, t.a.v. Ir. J.A. Vogel, daarna reserve
37. Archief TNO-FEL, in bruikleen aan M&P *)
38. Archief TNO-FEL, in bruikleen aan Prof.dr.ir. H. Dekker
39. Archief TNO-FEL, in bruikleen aan Dr.ir. A.M.J. van Eijk
40. Archief TNO-FEL, in bruikleen aan Drs. D. van Halsema
41. Archief TNO-FEL, in bruikleen aan Ir. A.N. de Jong
42. Archief TNO-FEL, in bruikleen aan Ir. J.C.M. Kleyweg
43. Archief TNO-FEL, in bruikleen aan Ir. G.J. Kunz
44. Archief TNO-FEL, in bruikleen aan Drs. C.W. Lamberts
45. Archief TNO-FEL, in bruikleen aan Dr. G. de Leeuw
46. Archief TNO-FEL, in bruikleen aan Mr. M.M. Moerman
47. Archief TNO-FEL, in bruikleen aan Dr.ir. H.M.A. Schleijpen
48. Archief TNO-FEL, in bruikleen aan Dr. P.B.W. Schwering
49. Archief TNO-FEL, in bruikleen aan Drs. B.J. van Dam
50. Archief TNO-FEL, in bruikleen aan Drs. J.P. Veeffkind
51. Documentatie TNO-FEL
52. Reserve

TNO-PML, Bibliotheek **)

TNO-TM, Bibliotheek **)

TNO-FEL, Bibliotheek **)

Indien binnen de krijgsmacht extra exemplaren van dit rapport worden gewenst door personen of instanties die niet op de verzendlijst voorkomen, dan dienen deze aangevraagd te worden bij het betreffende Hoofd Wetenschappelijk Onderzoek of, indien het een K-opdracht betreft, bij de Directeur Wetenschappelijk Onderzoek en Ontwikkeling.

*) Beperkt rapport (titelblad, managementuitreksel, RDP en distributielijst).

**) RDP.